JOURNAL OF GEOPHYSICAL RESEARCH, VOL. 115, D13203, doi:10.1029/2009JD013605, 2010

A three-dimensional characterization of Arctic aerosols from airborne Sun photometer observations: PAM-ARCMIP, April 2009

R. S. Stone,[1,2] A. Herber,[3] V. Vitale,[4] M. Mazzola,[4] A. Lupi,[4] R. C. Schnell,[2] E. G. Dutton,[2] P. S. K. Liu,[5] S.-M. Li,[6] K. Dethloff,[7] A. Lampert,[7,8] C. Ritter,[7] M. Stock,[7] R. Neuber,[7] and M. Maturilli[7]

Received 25 November 2009; revised 11 February 2010; accepted 4 March 2010; published 10 July 2010.

[1] The Arctic climate is modulated, in part, by atmospheric aerosols that affect the distribution of radiant energy passing through the atmosphere. Aerosols affect the surface-atmosphere radiation balance directly through interactions with solar and terrestrial radiation and indirectly through interactions with cloud particles. Better quantification of the radiative forcing by different types of aerosol is needed to improve predictions of future climate. During April 2009, the airborne campaign Pan-Arctic Measurements and Arctic Regional Climate Model Inter-comparison Project (PAM-ARCMIP) was conducted. The mission was organized by Alfred Wegener Institute for Polar and Marine Research of Germany and utilized their research aircraft, Polar-5. The goal was to obtain a snapshot of surface and atmospheric conditions over the central Arctic prior to the onset of the melt season. Characterizing aerosols was one objective of the campaign. Standard Sun photometric procedures were adopted to quantify aerosol optical depth AOD, providing a three-dimensional view of the aerosol, which was primarily haze from anthropogenic sources. Independent, in situ measurements of particle size distribution and light extinction, derived from airborne lidar, are used to corroborate inferences made using the AOD results. During April 2009, from the European to the Alaskan Arctic, from sub-Arctic latitudes to near the pole, the atmosphere was variably hazy with total column AOD at 500 nm ranging from ~0.12 to >0.35, values that are anomalously high compared with previous years. The haze, transported primarily from Eurasian industrial regions, was concentrated within and just above the surface-based temperature inversion layer. Extinction, as measured using an onboard lidar system, was also greatest at low levels, where particles tended to be slightly larger than at upper levels. Black carbon (BC) (soot) was observed at all levels sampled, but at moderate to low concentrations compared with historical records. BC was highest near the North Pole, suggesting there had been an accumulation of soot within the Arctic vortex. Few, optically thick elevated aerosol layers were observed along the flight track, although independent lidar observations reveal evidence of the passage of volcanic plumes, which may have contributed to abnormally high values of AOD above 4 km. Enhanced opacity at higher altitudes during the campaign is attributed to an accumulation of industrial pollutants in the upper troposphere in combination with volcanic aerosol resulting from the March–April 2009 eruptions of Mount Redoubt in Alaska. The presence of Arctic haze during April 2009 is estimated to have reduced the net shortwave irradiance by ~2–5 W m^{-2}, resulting in a slight cooling of the surface.

[1]Cooperative Institute for Research in Environmental Sciences, University of Colorado at Boulder, Boulder, Colorado, USA.
[2]Global Monitoring Division, Earth Systems Research Laboratory, National Oceanic and Atmospheric Administration, Boulder, Colorado, USA.
[3]Climate Sciences, Alfred Wegener Institute for Polar and Marine Research, Bremerhaven, Germany.
[4]Institute of Atmospheric Sciences and Climate, National Research Council, Bologna, Italy.
[5]Meteorological Research Division, Environment Canada, Toronto, Ontario, Canada.
[6]Air Quality Research Division, Science and Technology Branch, Environment Canada, Toronto, Ontario, Canada.
[7]Research Unit Potsdam, Alfred Wegener Institute for Polar and Marine Research, Potsdam, Germany.
[8]Now at Institute of Aerospace Systems, Technische Universität Braunschweig, Braunschweig, Germany.

0148-0227/10/2009JD013605

Citation: Stone, R. S., et al. (2010), A three-dimensional characterization of Arctic aerosols from airborne Sun photometer observations: PAM-ARCMIP, April 2009, *J. Geophys. Res.*, *115*, D13203, doi:10.1029/2009JD013605.

1. Introduction

[2] The Arctic was once thought to be a pristine environment. As early as 1870, however, *Nordenskiöld* [1883] found anecdotal evidence that the Arctic was being contaminated by pollutants transported from lower latitudes [*Hirdman et al.*, 2009]. During the 1950s, U.S. pilots on reconnaissance flights into the Arctic reported seeing layers of pollutants [*Mitchell*, 1957]. The phenomenon was thereafter referred to as Arctic haze, thought to be composed of soot, dust, and sulphates emitted by industrial complexes located in Eurasia, transported into the Arctic during winter and spring [*Shaw*, 1995]. Haze is known to perturb the Arctic surface-atmosphere radiation balance [e.g., *Shaw and Stamnes*, 1980; *Blanchet*, 1989]. In general, quantification of the direct and indirect impacts of aerosols on climate remains an outstanding problem [*Intergovernmental Panel on Climate Change* (*IPCC*), 2007]. In particular, the Polar regions present challenges owing to peculiarities related to large variations in aerosol concentration, distribution, chemical, physical and optical properties, complicated by dramatic seasonal changes in solar geometry and surface albedo. Quantification of the direct radiative forcing by different types of Arctic aerosol using empirical methods has been demonstrated [*Stone et al.*, 2007, 2008], but case studies have been few and limited in scope thus far. In addition, aerosols nucleate and/or interact with cloud particles to affect their microphysical and radiative properties [*Twomey*, 1977; *Kaufman and Fraser*, 1997], which further modulates the radiation budget of the region. More in-depth monitoring and analyses are required to better characterize the mixtures of aerosols observed in the Arctic and their impact on that fragile environment. For instance, black carbon (soot) particles may enhance atmospheric warming [e.g., *Warneke et al.*, 2009; and references within], contributing to the decline of Arctic sea ice [*Stroeve et al.*, 2007]. In addition, the deposition of soot onto the ice/snow surface can reduce albedo, increase solar absorption and further accelerate melting [e.g., *Flanner et al.*, 2007; *Clarke and Noone*, 2007]. These warming effects compete with aerosol layers that primarily backscatter sunlight and cool the surface. The direct and indirect effect of aerosols, coupled with the diverse boundary layer conditions and dramatic annual solar cycle that characterize the Arctic system, make it difficult to assess their net climatic impact. A goal of PAM-ARCMIP was to characterize the Arctic aerosol. The campaign was organized by the Alfred Wegener Institute for Polar and Marine Research (AWI) of Germany with support of the international community. AWI also provided the Polar-5 research aircraft, a Basler BT-67, for the mission.

[3] The campaign was conducted between 1 April and 25 April 2009 (http://www.sciencecentric.com/news/article.php?q=09050433-research-aircraft-polar-5-finishes-arctic-expedition) as the first of a planned series of Arctic circum-navigations. The goal of the project is to collect comprehensive data sets needed to better understand the Arctic climate system, how it is changing and ostensibly to understand processes that determine sea ice distributions. The mission was conceived logistically and scientifically to take advantage of existing climate observatories in the Arctic, where long-term observations have been made for comparative analyses. Also, timed with the culmination of the International Polar Year (2007/2009), the intent was to begin a legacy project involving repeated circum-Arctic navigations using research aircraft. The measurements will be interpreted and used as input to regional climate models to simulate the Arctic climate following the approach of *Rinke et al.* [2006]. An earlier study using a regional atmospheric model revealed large variations due to the impact of aerosols, depending on the surface albedo, atmospheric humidity, and cloud distributions [*Rinke et al.*, 2004].

[4] During PAM-ARCMIP, measurements of sea ice thickness, ozone and mercury, aerosol, including optical depth, particle size distributions, black carbon concentration, radiative fluxes and atmospheric state variables were made. One objective was to characterize the aerosol horizontally and vertically using standard photometric procedures. Similar characterizations were made during earlier aircraft campaigns, as early as the 1980s, described in special issues of *GRL* and *J. Atmos. Chem.* [e.g., *Schnell*, 1984; *Schnell et al.*, 1989] and as recently as the spring of 2008 [e.g., *Warneke et al.*, 2009]. In between, there were several international campaigns focused on the study of Arctic aerosols as well [e.g., *Skouratov*, 1997; *Shiobara et al.*, 1999; *Yamanouchi et al.*, 2003, 2005; *Arnold et al.*, 2009]. The Arctic Airborne Measurement Program (AAMP) flights in 1998 and 2002 both flew over the North Pole and provided rare observations of the stratospheric aerosol burden. Despite the collective efforts over the decades, there remain large uncertainties in quantifying the radiative effects of aerosols [*IPCC*, 2007]. In the Arctic, not only the magnitude but the sign of the forcing may vary, depending on aerosol composition, cloud interactions, solar geometry and underlying surface conditions [e.g., *Stone et al.*, 2008, Figure 10]. Better characterizations of Arctic aerosol properties, particularly optical depth, are required in order to quantify their direct radiative impacts on climate. The focus of this study is to quantify the AOD of aerosols present in the Arctic atmosphere during April 2009, a time of year known to be influenced by long-range transport of pollutants from lower latitudes. In particular, properties of Arctic haze are characterized, as derived from Sun photometer observations and ancillary measurements. Papers describing the other observations made during the campaign and their analyses are in various stages of preparation. Note that in addition to this manuscript, auxiliary material is available online, in the form of a visual slide show and one video clip.[1]

2. Measurements

2.1. PAM-ARCMIP Sun Photometer Observations

[5] The derivation of spectral AOD from PAM-ARCMIP Sun photometer observations follow the widely accepted

[1] Auxiliary materials are available in the HTML. doi:10.1029/2009JD013605.

practice of inverting the Bouguer-Lambert-Beer law that expresses the attenuation of direct solar radiation passing through the atmosphere. The methods employed follow those outlined by *Stone* [2002, and references therein].

[6] Spectral AOD data were derived from measurements made using an 8-channel Sun photometer system developed by investigators at the U. S. National Oceanic and Atmospheric Administration (NOAA) and the Institute of Atmospheric Sciences Climate-National Research Council (ISAC-CNR), Italy. This was interfaced with a solar tracker (model SPTRV5) provided compliments of the company, Dr. Schulz and Partners, Germany. The system was integrated into Polar-5 on the left, forward side of the cabin. A B270 Superwite® glass pane replaced the original window at that station, which was carefully characterized for its spectral transmissivity over a range of view angles (<25° relative to perpendicular). On command, the data acquisition system recorded spectral irradiance at nominal, central wavelengths of 368, 412, 500, 610, 675, 778, 862 and 1050 nm at one-second resolution, along with GPS position and altitude along the flight track. Data were collected for all clear-sky periods when the sun was within 25 degrees of perpendicular to the flight track (and during periods of thin cloud for future study). Nearly 88,000 individual AOD spectra were recorded during the campaign. Along track, observations were made with a horizontal resolution of about 50 m and in the vertical, approximately 5 m. Observations were made from near the surface, 60 m, to an altitude of ~4000 m when profiling. During ferry flights measurements were made between 2850 m and 3250 m.

2.1.1. Cloud Screening of PAM-ARCMIP AOD Data

[7] All AOD data analyzed subsequently were screened to minimize the influence of thin clouds. Objective cloud screening of photometric data is never perfect, often involving subjective selection of thresholds used to distinguish aerosol from cloud. A few thin clouds may pass through screening while some inhomogeneous aerosol layers may be eliminated in the process. No one algorithm has been universally adopted. Indeed, this may not be wise because aerosol/cloud regimes differ geographically and an approach suited to mid latitudes may not work well in the central Arctic. In general, clouds exhibit much higher temporal-spatial variability than do aerosols. This distinction is the basis of most cloud-screening algorithms. For our purposes we screened data two ways and compared the results.

[8] At the NOAA Earth System Research Laboratory-Global Monitoring Division (ESRL-GMD), a method has been adopted to exploit the difference in temporal variability between cloud and aerosol optical depths, by analyzing successive groups of 11 observations to determine their range and indentify points falling outside a set threshold as being contaminated by the presence of cloud. The test is applied to the midpoint of each group, before advancing one time step. GMD normally processes one-minute data from its baseline observatories. Here, the same algorithm was applied to the one-second aircraft data. Flying at a speed of ~50 m s^{-1}, we successively evaluated variations over a distance of ~600 m. As with other methods, the choice of threshold determines the likelihood of clouds escaping detection or aerosols being eliminated. Thresholds are selected on the basis of experience and are site specific. In the case of the PAM-ARCMIP analysis, we used the same threshold value, 0.015, used operationally to screen one-minute data from Barrow, Alaska, Alert, Canada and South Pole, Antarctica.

[9] The second approach, applied by the group at ISAC, employed a procedure similar to that of *Alexandrov et al.* [2004], again exploiting the fact that temporal variations in aerosol optical depth tend to be much lower than for clouds. In this case, variability is quantified by an in homogeneity parameter ε. As the plane passes below an aerosol layer, ε will have lower values then below a cirrus cloud, for example.

[10] The ISAC method follows: each value of AOD was rescaled by subtracting the running mean of 12 adjacent data points and adding a typical value observed during the campaign, taken to be 0.20. This results in a new time series having more constant value but maintaining the original variations. Successive tests are then made to determine if the standard deviations σ of running averages exceeds a threshold value. Here we require σ to be <0.04 to pass as aerosol. Again, the procedure is applied successively, stepping through the time series.

[11] In both procedures each wavelength was analyzed separately and then the spectral values were recombined. The spectral data were further evaluated to eliminate points suspected of being clouds by virtue of having abnormally high values of AOD and/or spectral signatures more typical of cloud than of aerosol. This is illustrated by *Treffeisen et al.* [2007, Figure 7] wherein values of the Ångström exponents Å(412/675) for cirrus-type clouds have low or negative values compared with most types of aerosol. On the basis of observations made during PAM-ARCMIP, comparing signatures of observed thin cirrus and clear-sky aerosols, we selected AOD(500) $\leq$ 0.40 as an upper limit and required Å(412/675) be $\geq$0.38 to pass as aerosol. While these restrictions are not generally applicable, they were determined to be reasonable during this particular campaign as a means to cloud-screen the AOD data in a consistent way. Furthermore, when examined statistically the two independent analyses (NOAA versus ISAC) yielded essentially the same statistical results, giving credence to both methods.

2.1.2. Polar-5 Flight Track and Sun Photometer Data Collection

[12] Figure 1 shows the flight track (blue) and where photometric observations were made (red) during PAM-ARCMIP. Ground stations are identified by name in the table (inset) and the approximate locations of 15 profiles are indicated on the map. The profiles are numbered in accordance with flight segments listed in Table 1, by date, nearest degree of latitude and longitude, and location relative to the nearest ground station, by identifier. A partial drift track of the SHEBA (Surface Heat Budget of the Arctic Ocean) ice camp during spring 1998 [*Uttal et al.*, 2002], and the Russian drifting station, NP-35, during 2008 are also indicated. Unfortunately, no clear-sky observations were made above about 4000 m during the campaign. Therefore, characterization of the upper-level AOD can only be estimated (section 3.6).

[13] The photometer system used during PAM-ARCMIP is similar in design to those operating at Barrow, Alaska (BRW), Alert, Canada (ALT) and at South Pole (SPO), Antarctica. Each is thermally controlled to maintain opera-

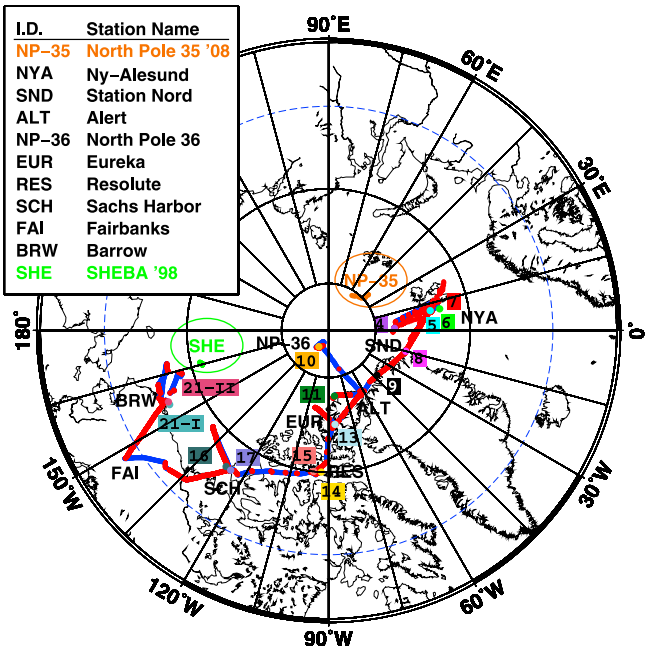

Figure 1. Map view of the Polar-5 flight track during PAM-ARCMIP (blue) and locations of all Sun photometer observations made during the campaign (red). The encircled orange trace is where AOD measurements were made in March–April 2008 at the Russian drifting station, NP-35, and the encircled green trace indicates where similar measurements were made during SHEBA in spring 1998. The key (inset) assigns station identifiers to their respective names, following counterclockwise from NP-35. The numbers refer to profiles made during the campaign, listed in Table 1. The dashed blue line indicates the Arctic Circle.

tion at approximately the same temperature that it was calibrated at. Calibrations performed at the NOAA Mauna Loa Observatory (MLO) and processing procedures followed those described by *Stone* [2002]. The system used during PAM-ARCMIP was calibrated at the Izaña Observatory, Tenerife, Canary Islands using the same methodology. On the basis of results obtained at the Izaña inter-calibration campaign, October 2008 (M. Mazzola et al., Evaluation of Sun photometer capabilities for the retrievals of aerosol optical depth at high latitudes: The POLAR-AOD project, manuscript in preparation, 2010), the accuracy of AOD retrievals obtained during PAM-ARCMIP are estimated to be within ±0.005 for wavelengths in the range 412 nm to 862 nm and somewhat less accurate at 368 nm and 1050 nm owing to lower signal-to-noise ratios and possible thermal effects. To achieve this level of accuracy requires corrections be made for ozone and NO_2 attenuation, in particular at wavelengths of 500, 610 and 675 nm for ozone and 412 and 500 nm for NO_2. In this case, corrections were made on the basis of satellite-derived column ozone and NO_2 amounts. Values were extracted to coincide with the mid point of each flight segment as retrieved by the Ozone Monitoring Instrument (OMI) on board the Aura satellite; for ozone, OMITO3: http://toms.gsfc.nasa.gov/omi/and for NO_2, http://avdc.gsfc.nasa.gov/index.php?site=705441739.

[14] Globally, OMI-TOMS retrievals of column ozone amounts are accurate to within about 2%, based on validation studies performed using surface measurements [*Balis et al.*, 2007]. To account for an approximate 5% decrease in ozone from the surface to 4 km, corrections were applied as a function of flight altitude before computing ozone optical depths. The OMI NO_2 product is not so accurately derived, however. *Celarier et al.* [2008] found that the OMI retrievals of total column NO_2 are reasonably correlated with ground-based measurements but are biased low by as much as 30%. On this basis, we scaled the retrievals obtained for each flight segment by a factor of 1.28 and account for an approximate 2% decrease in column amount from the surface to 4 km. Because NO_2 is highly variable and our scaling is somewhat arbitrary/uncertain, estimates of NO_2 optical depth used in the analysis are probably no better than ±10–15%. No matter, these lead to uncertainties in AOD of <0.003 in the worst case. Uncertainties in AOD due to erroneous ozone corrections are <0.001 [*Mazzola et al.*, 2010].

[15] Finally, gaseous absorption coefficients were derived, by wavelength, using the MODTRAN™ radiative transmission code [e.g., *Berk et al.*, 2004] for a model winter atmosphere.

Table 1. Vertical Profiles, By Flight Number, Made During PAM-ARCMIP[a]

Flight Number	Date (UT)	Day of Year (UT)	Latitude (°N)	Longitude (deg, +E; −W)	Altitude Range (m)	Nearest Station
04	3 April	93	83	+01	145–3910 (*A*)	NYA
05	4 April	94	79	+11	3920–075 (*D*)	NYA
06	5 April	95	79	+11	3980–060 (*D*)[b]	NYA
07	6 April	96	78	+16	3970–070 (*D*)[b]	NYA
08	8 April	98	82	−14	3010–120 (*D*)	SND
09	9 April	99	83	−45	2900–120 (*D*)	ALT
10	10 April	100	88	−121	005–2050 (*A*)	NP-36
11	11 April	101	83	−85	2740–90 (*D*)	ALT
13	13 April	103	80	−86	3775–060 (*D*)[b]	EUR
14	14 April	104	75	−94	3890–080 (*D*)	RES
15	15 April	105	75	−96	445–3180 (*A*)	RES
16	16 April	106	72	−125	3980–200 (*D*)[b]	SCH
17	17 April	107	72	−125	775–3000 (*A*)	SCH
21-I	24 April	114	71	−157	390–2905 (*A*)	BRW
21-II	25 April	115	71	−156	3920–60 (*D*)	BRW

[a]To cross reference with the flight track shown in Figure 1 and analyses presented in Figure 7. Each is denoted as an ascent (*A*) or descent (*D*), in parentheses besides the altitude range.
[b]Observations made at discrete altitudes during descent, rather than continuously.

2.2. Lidar Extinction Profiles

[16] Complementary measurements were made using lidars, operating on Polar-5 and at ground stations along the route. On board was the Airborne Mobile Aerosol Lidar (AMALi) system, developed by AWI-Potsdam, which operates at wavelengths of 532 nm and 355 nm [*Stachlewska et al.*, 2009]. Processed data includes 7.5 m vertically resolved profiles of 532 nm volume extinction (km^{-1}) and linear depolarization ratio. It utilizes an Nd:YAG pulsed laser. While it can be operated pointing up or down, during the campaign it was directed downward in the nadir position to obtain profiles below cruising altitudes, generally below 2800 m. Using nearly coincident AOD data as a means to calibrate AMALi retrievals, highly resolved profiles of volume extinction were obtained.

[17] The Koldewey Aerosol Raman Lidar (KARL) is operated at Ny-Ålesund, NYA (78.9°N, 11.9°E), also by AWI. It was designed to measure aerosol and water vapor. The system uses the elastic wavelengths of 355 nm, 532 nm and 1064 nm and the inelastic Raman shifted lines of N_2 at 387 nm and 607 nm for deriving extinction measurements [*Ansmann et al.*, 1992], and at 407 nm to retrieve water vapor amounts. A short description of the system is given by *Hoffmann et al.* [2009]. It includes a newly designed, movable aperture that enables scanning from near the surface into the stratosphere. During PAM-ARCMIP, this aperture was adjusted in a way to produce profiles from about 500 m to more than 20 km in altitude.

[18] In addition, time-height cross sections of lidar backscattering coefficients retrieved from the University of Wisconsin Arctic High Spectral Resolution Lidar (AHSRL) at Eureka, Canada (80.0°N, 85.9°W) [*Eloranta*, 2005] and the U.S. Department of Energy (DOE) micro pulse lidar (MPL) at Barrow, Alaska (http://www.arm.gov/sites/nsa.stm) were used to visually evaluate characteristics of aerosol at mid to upper levels of the atmosphere. In particular, the AHSRL was useful for comparing general extinction characteristics during April 2009 with those of April 2008.

[19] Finally, Cloud-Aerosol Lidar and Infrared Pathfinder Satellite Observation (CALIPSO) browse images for expedited release by NASA (http://www-calipso.larc.nasa.gov/products/lidar/browse_images/show_calendar.php) were examined for near-coincident overpasses relative to the flight track of Polar-5, to compare aerosol observations and to evaluate stratospheric events that may be related to volcanic aerosol plumes.

2.3. Ancillary Measurements Made on Board Polar-5

[20] Condensation nuclei (CN) and particle size distributions were measured by Environment Canada (EC) operators on board Polar-5. Aerosols were sampled via a diffuser type air inlet with flow maintained as close as possible to isokinetic conditions. CN concentrations were measured with a PMS condensation nucleus counter, model CN7610, which has a lower detection limit of 14 nm diameter.

[21] Aerosol size distributions were measured using an Ultra High Sensitivity Aerosol Spectrometer (UHSAS) [*Cai et al.*, 2008] manufactured by Droplet Measurement Technology. The particle size range measured was from 60 to 1000 nm diameter in 99 channels.

[22] Black carbon BC (soot) concentrations were measured using the EC single-particle soot photometer, SP2. The SP2 uses laser incandescence to detect individual soot particles in sampled air. BC concentrations measured by this device compare reasonably well with those measured by an Aerosol Mass Spectrometer and Scanning Mobility Particle Sizer (AMS-SMPS), or a Photoacoustic Spectrometer (PAS) [*Slowik et al.*, 2007]. For uncoated soot particles, the agreement is within ~10%, thus the SP2 measurements provide a reliable record of BC throughout the campaign. Several profiles were obtained to evaluate BC concentrations in the vertical for comparisons with historical aircraft and ground-based measurements.

[23] During several flight legs, dropsondes were launched to measure atmospheric state variables using a system developed by Vaisala. RD93-type sondes measured pressure, temperature, relative humidity and wind seed and direction from about 3500 m altitude to the surface, transmitting data to a receiving system onboard Polar-5. In all, 59 sondes were launched to characterize the vertical thermal, dynamical and moisture structure of the Arctic atmosphere. In particular, these are used here to determine the depth and strength of the surface-based temperature inversion for regimes that differ with latitude and surface conditions, and also to evaluate relative humidity relative to particle sizes observed.

3. Analyses

3.1. Overview of Synoptic and Airflow Patterns During PAM-ARCMIP

[24] During April 2009 large-scale circulation patterns affecting airflow in the Arctic evolved over time, as illustrated in Figure 2, which shows weekly mean 850 hPa geopotential height fields from National Centers for Environmental Prediction (NCEP) gridded data; http://www.esrl.noaa.gov/psd/data/gridded/reanalysis. Back-trajectories are drawn schematically to show transport pathways corresponding to the NCEP 850 hPa vector wind fields (not shown). The trajectories are shown relative to NYA (Ny-Ålesund, Svalbard), NP-36 (the Russian North Pole, drifting station) and BRW (Barrow, Alaska).

[25] At the beginning of the campaign NYA was influenced by a flow of relatively clean air from the Canadian Arctic, passing over the Greenland ice cap (Figure 2a). By 10 April, when Polar-5 flew nearest the Pole, the Kara Sea ***L*** had combined with the European ***H***, which established a pattern favoring flow from Eurasia, eastward across the industrial regions of northern Russia, then northward (Figure 2b). This is a common pathway for pollutants to enter the central Arctic [e.g., *Raatz*, 1989; *Yamanouchi et al.*, 2005; *Hirdman et al.*, 2009, 2010]. Transit times were estimated to be 4–7 days, based on forward trajectory analyses provided by J. Harris of NOAA/GMD. By the end of the campaign, when flying in the vicinity of Barrow, the large-scale circulation had changed significantly. The low over northern Siberian had expanded further and appears to have merged with the Aleutian Low over the North Pacific, which coupled with an intense high pressure ridge over Alaska. The pattern favored long-range transport from western Russian, dipping south through eastern Asia around the Aleutian Low, entering the Alaskan Arctic as shown in

Figure 2c. Such flow, through a deep layer, might entrain a variety of different aerosols before passing over BRW, including industrial pollutants from Eurasia, dust from a massive storm over the Taklimakan Desert on 17–19th April, 2009 (http://earthobservatory.nasa.gov/NaturalHazards/view.php?id=38263); and possibly volcanic aerosols from ongoing eruptions of Mount Redoubt in Alaska, as reported by the Alaska Volcano Observatory (http://www.avo.alaska.edu/).

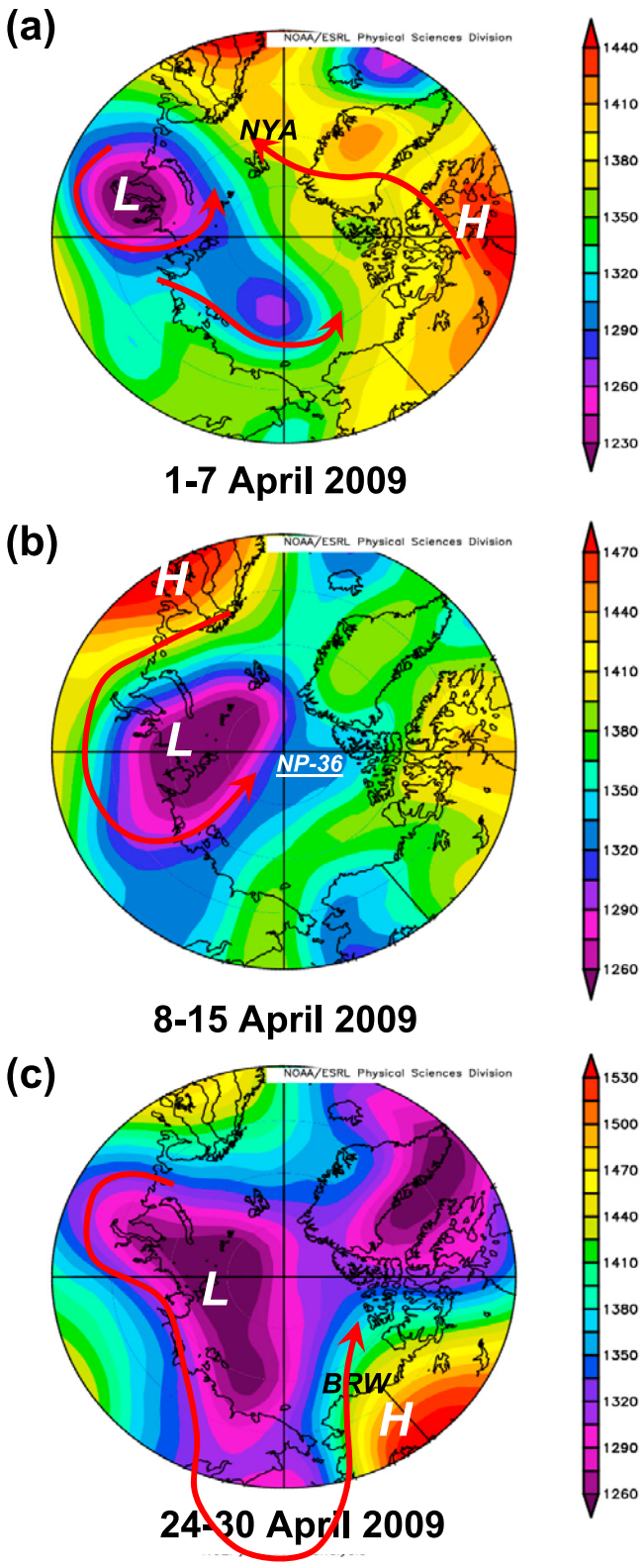

3.2. Overall Characteristics of Arctic Aerosols During April 2009

[26] The fundamental measurement from which values of AOD are derived is transmitted direct beam solar irradiance, resolved spectrally by the Sun photometer. Similar observations were made in the early 1980s [*Spinhirne and King*, 1985] during AGASP missions using simple, hand-held photometers [*Dutton et al.*, 1989; *Stone et al.*, 1993]. Sun photometry has improved over time as more automated systems have been developed [e.g., *Skouratov*, 1997; *Yamanouchi et al.*, 2005]. With advancements in technology it is now possible to collect much higher resolution data from aircraft. For example, the NASA Ames Airborne Tracking Sun photometer (AATS) has 14 channels ranging from 354 to 2139 nm with robotic tracking in azimuth and elevation using motors controlled by differential sun sensors [*Russell et al.*, 2005], http://geo.arc.nasa.gov/sgg/AATS-website/.

[27] PAM-ARCMIP provided the opportunity to assimilate a comprehensive, highly resolved set of AOD profiles and horizontal transects covering a vast region of the Arctic during the peak of the 2009 haze season. The aircraft data are of high quality as evidenced by comparison with nearly coincident surface-based measurements shown in Figure 3. Validation points were located at Ny-Ålesund at the beginning of the campaign, Alert midway through, and at Barrow at the end, representing different climate regimes, a broad geographical area and a range of optical depths. Each station calibrates and processes its data independently. Overall, there is very good agreement between the aircraft and surface spectral signatures and absolute values in the wavelength range 412–862 nm. The average differences are <0.005, the accuracy of any one system operating independently and show no bias. As mentioned above, the 368 nm and 1050 nm channels are prone to greater error and therefore differ slightly more. The excellent agreement attests to the fact that corrections for glass transmission, gaseous absorption and molecular scattering were all correctly applied to the aircraft data.

[28] The rather persistence pattern of atmospheric circulation (Figure 2) established in early April is believed to have contributed significantly to the aerosol distribution measured throughout the campaign. There was no apparent influence of forest fire smoke as was the case the previous April [*Warneke et al.*, 2009]. The pervasiveness of the haze was confirmed by AOD measurements that were made

Figure 2. Mean weekly geopotential fields at the 850 hPa pressure level for the Arctic for (a) 1–7 April, (b) 8–15 April, and (c) 24–30 April 2009 showing the main synoptic features that determine the atmospheric general circulation at respective times. The red arrows represent, schematically, the 850 hPa vector wind analyses (not shown) relative to locations and timing of Polar-5 flights near ground stations indicated during PAM-ARCMIP (see also Figure 1 and Table 1). The fields were generated using NCEP gridded data made available through the NOAA/-ESRL Physical Sciences Division (PSD) at: http://www.esrl.noaa.gov/psd/.

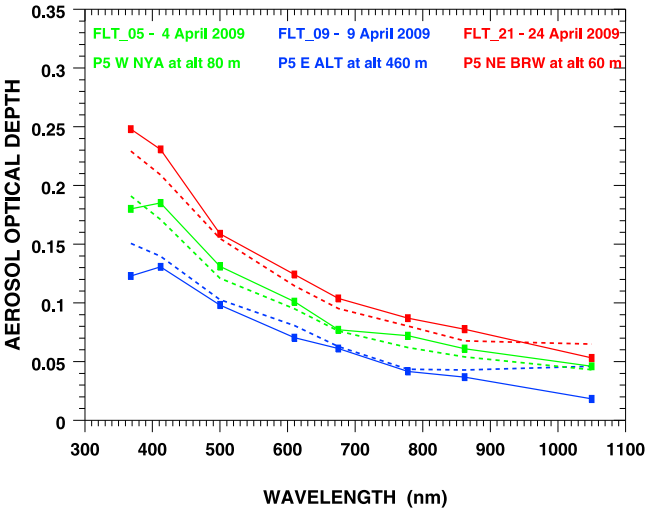

Figure 3. Comparisons between aircraft (solid curve) and ground-based (dashed curve) measurements of spectral aerosol optical depth made at nearly coincident times at three locations during PAM-ARCMIP. Flight numbers, dates, and locations are indicated in the legends and can be cross-referenced to Figure 1. Note that the sublegends give information about the proximity of Polar-5 (P5) to the nearby ground station, by compass direction and altitude.

during the traverse from Svalbard to Point Barrow (Figure 1). AOD values at 500 nm AOD(500) ranged from about 0.12 to 0.40 for all observations made below 160 m, compared with typical background values that range for 0.04–0.06. Similar analyses were carried out for measurements made at cruising altitudes (2850 m < alt < 3250 m) and at the highest altitudes flown (>3750 m). The observations were made within about a three week period, 2–24 April 2009, during which time Polar-5 traversed roughly 190 degrees of longitude, within a latitude band between 65° and 88°N. The horizontal distributions, magnitudes and relative frequency plots of AOD(500) are shown in Figure 4. In general, the air was less turbid at low and mid levels during the first several days of operation, east of Alert, and more turbid during the westward flight from Alert, particularly in the eastern Beaufort region. This produced the bimodal relative frequency distribution of AOD(500) shown in Figure 4b. The modes relate to the changing synoptic patterns that were described above in relation to Figure 2. While fewer observations were made at the highest levels (Figure 4e), they are representative of a broad region of the Arctic. Here we find a sharp peak in distribution of AOD(500), centered at about 0.05, with slightly higher values in the vicinity of Pt. Barrow, features discussed in a following section.

[29] Figure 5a shows time series of daily means of AOD (500) from six ground stations from mid March to mid May, 2009 (day of year 75–135). Figure 5b is an ensemble of similar time series from Barrow and Ny-Alesund (2006–2008), Alert (2006 and 2007), from the SHEBA ice camp (1998) and the Russian drifting station, NP-35 (2008). The location of each site can be cross-referenced with Figure 1. The lower, dashed line represents the upper limit of clean background air. To contrast the broad-scale turbidity of the central Arctic in 2009 with the previous three years, composite average data for Alert, Barrow and Ny-Ålesund are smoothed using a seven-day filter in Figure 5a and similarly for the ensemble of 8-station years in Figure 5b, indicated in each by a bold black curve. In Figure 5b, the 2009 smoothed series is shown again as a dashed line for comparison. It is clear that during PAM-ARCMIP the Arctic atmosphere was significantly more turbid than in the previous three years when averaged in this manner. On average, the SHEBA 1998 and NP-35 2008 data fall within the ensemble. In 2009, AOD peaked anomalously during mid April 2009 but in May began to diminish, which is typical as the Arctic vortex begins to weaken and break up. Although a climatology of AOD for the central Arctic has not yet been established, this limited analysis suggests that 2009 was anomalously turbid. We attribute this to the persistence of the particular flow pattern shown in Figure 2 that favored the transport of industrial pollutants into the Arctic from Eurasia, further enhanced by upper-level incursions of volcanic aerosol and possible contributions from coal burning in China, as will be discussed further in section 3.6.

[30] Monitoring the overall turbidity of the Arctic atmosphere (during the sunlit portion of the year) may soon be possible in this manner by combining all AOD observations from a network of Arctic ground stations operating Sun photometers [*Tomasi et al.*, 2007], including those established in recent years by NASA as part of its AErosol RObotic NETwork AeRoNET (http://aeronet.gsfc.nasa.gov/) [*Holben et al.*, 1998]. Data from Andenes, Norway (69.3°N, 16.3°E) and Hornsund, Svalbard (77.0°N, 15.7°E) shown in Figure 5a are from AeRoNet. Others to include are Eureka, Canada, three locations in Greenland, and beginning in 2010, Tiksi, Russia (71.6°N, 128.9°E). It is clear that each year will vary as is evident in Figure 5. Changes in aerosol composition related to emission rates and seasonal circulation patterns will be assessed using dispersion models [e.g., *Hirdman et al.*, 2010] and results can be compared with satellite retrievals and in situ aircraft data.

[31] In addition to quantifying AOD(500) the photometric data were used to determine spectral signatures, from which relative particle sizes can be inferred. This was done for the three respective flight levels, as shown in Figure 6. A log scale is used to demonstrate how Ångström exponents $\mathring{A}$ were evaluated from values of AOD at 412 nm and 675 nm using the relationship

$$\mathring{A}(412/675) = -\log 10(\mathrm{AOD}(412)/\mathrm{AOD}(675))/\log 10(412/675) \quad (1)$$

Ångström exponents are related inversely to mean particle size [*Ångström*, 1929], assuming the power law is a valid representation of spectral optical depth [*Ångström*, 1964]. Values of $\mathring{A}$ are also useful for distinguishing the relative fraction of fine to coarse mode particles in mixtures of aerosols [*Kaufman et al.*, 1994; *O'Neill et al.*, 2001; *Saha et al.*, 2010]. The method of *O'Neill et al.* [2001] exploits the naturally occurring curvature in the spectral AOD to resolve a fine particle mode and optical fraction of the fine particles in the aerosol. Such an analysis of the PAM-ARCMIP data is the subject of another paper and will not be discussed here. In our simplistic approach, values of Å(412/675) ≤1.0

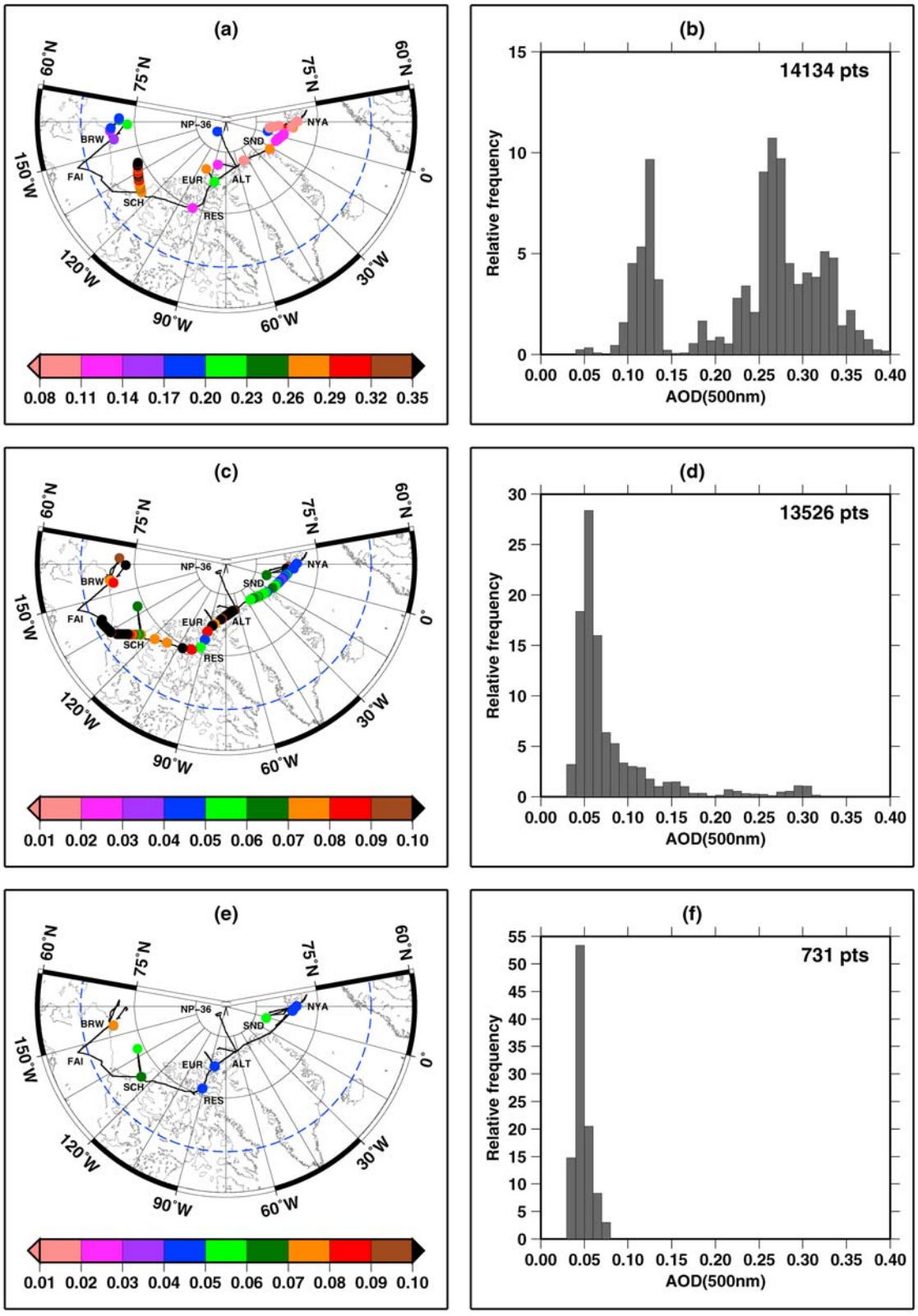

Figure 4. Maps showing the locations where AOD retrievals were obtained during PAM-ARCMIP at (a) low levels (alt < 160 m), (c) cruising altitudes (2850 m < alt < 3250 m), and (e) levels above 3750 m. Values of AOD(500) are plotted according to the respective color scales, and (b, d, and f) corresponding histograms of relative frequency of AOD(500) values, with the number of observations analyzed indicated.

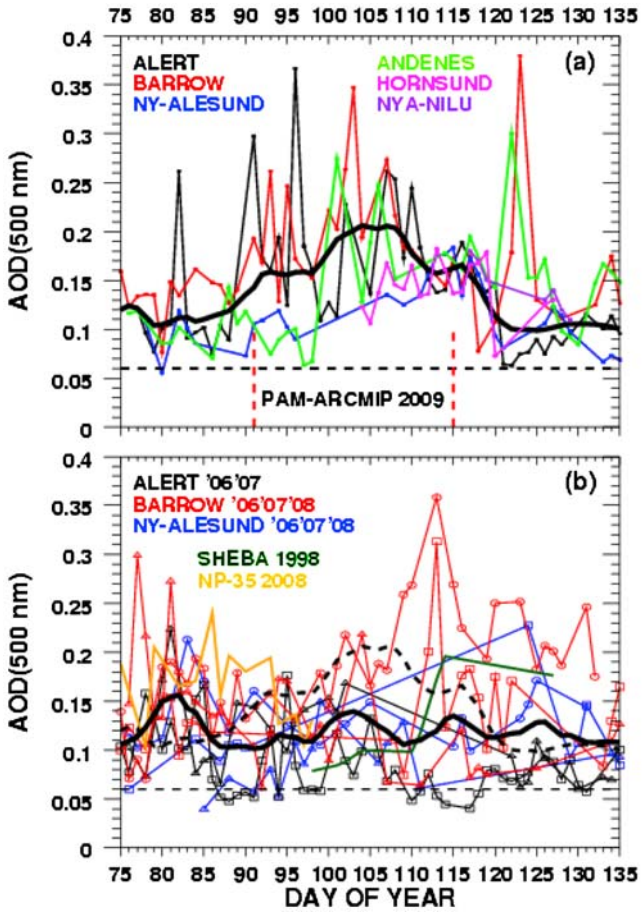

Figure 5. (a) Time series of mean daily values of AOD (500), mid March to mid May 2009, at Alert, Barrow, and Ny-Ålesund, smoothed as an ensemble, shown in bold black. Similar data from the AeRoNet sites, Andenes, Norway and Hornsund, Svalbard, and another site at Ny-Ålesund operated by NILU (Norwegian Institute for Air Research) are shown for comparison. (b) Similar daily mean time series for Alert (2006 and 2007), Barrow (2006–2008), and Ny-Ålesund (2006–2008), smoothed as an ensemble, shown in bold black compared with the dashed black curve from Figure 5a for comparison. Open squares, triangles, and circles represent data for 2006, 2007, and 2008, respectively. Also plotted in Figure 5b are data from the North Pole Russian drifting station NP-35 for 2008 and data from the SHEBA ice camp in 1998 (encircled in Figure 1). The lower, dashed line represents the upper range of clean atmospheric conditions observed typically during the Arctic spring. PAM-ARCMIP took place from DOY 91 to 115. All analyses are restricted to clear-sky periods; thus the data gaps.

and ≥1.5 are considered indicative of large and small particle dominance, respectively. Dust particles for instance tend to have smaller values [*Treffeisen et al.*, 2007], while smoke particles have much higher values [*Stone et al.*, 2008]. We find that values measured during PAM-ARCMIP systematically increase with altitude; that is, the largest particles tend to reside at the lower levels.

3.3. Vertical Structure of the Aerosol During April 2009

[32] To investigate how aerosols are distributed in the vertical, a number of profiles were flown between 60 and 4000 m; not all were complete, however. Five of these were made during ascents and 10 during descents (Table 1). Four of the descents were made while spiraling, flying horizontal legs at 11 discreet levels of which seven were below 1000 m to resolve the low-level variations in AOD. Profiling presented opportunities to collect comprehensive data sets of many variables, including AOD, broadband irradiance, particle size spectra, CN and BC concentrations, and ozone and mercury concentrations for comparative analyses. Here the focus is on AOD and derived parameters, mean geometric size, CN and BC. Where possible, lidar-derived volume extinction coefficients are compared with those derived from photometric measurements (in section 3.5).

[33] In addition to deriving values of $\mathring{A}$(412/675), profiles of mean layer volume extinction coefficient $K_{ext}(\Delta z)$ were derived using the following expression;

$$K_{ext}(\Delta z) = AOD(\Delta z)/\Delta z \quad (2)$$

where Δz is the geometric thickness of the layer and AOD (Δz) is the layer average optical depth.

[34] To simplify presentations, data are averaged into 200 m thick layers. Typically, the profiles took about 20–25 min to complete, during which time Polar-5 traversed about 60 to 80 km, depending on ground speed. On this scale, aerosol concentrations can vary horizontally as well as in the vertical. Therefore, profiles obtained are only approximations of the true vertical structure. At times during an ascent, for instance, higher values of AOD may be measured above a given level than below it; a non-physical condition

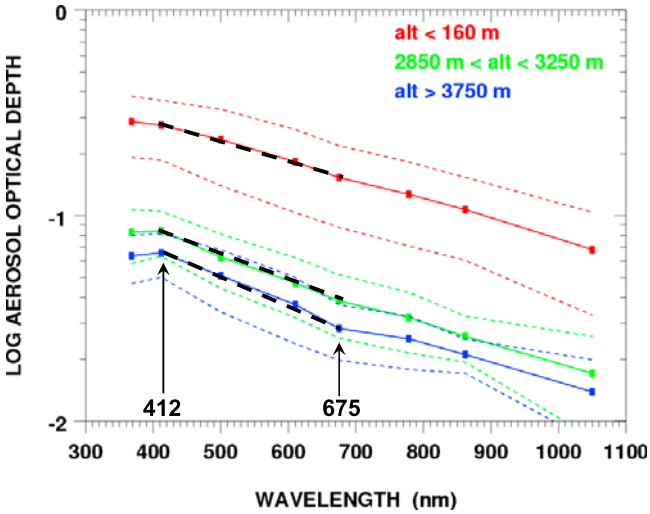

Figure 6. Mean spectral AOD as measured for the atmospheric column above three levels defined according to the legends. Also shown, schematically, are analyses of Ångström exponents Å(412/675) used to infer relative size of particles in the respective columns. Steeper slopes are indicative of smaller particles.

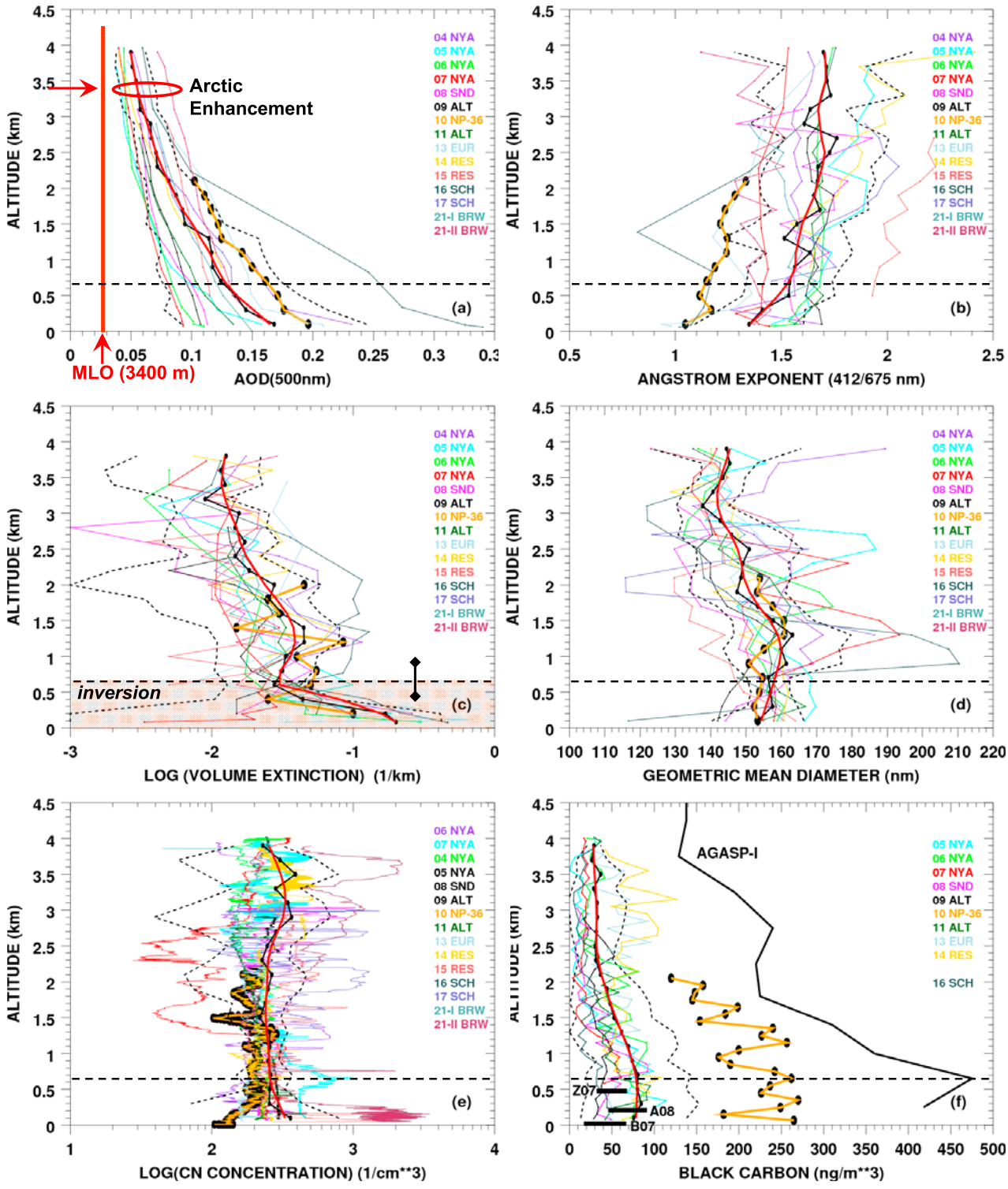

Figure 7

that can result in negative values of extinction (equation (2)). Averaging eliminated this issue.

[35] Figure 7 summarizes results composited from 15 individual profiles flown over the course of the campaign. Their approximate locations, by flight number, are indicated in Figure 1 and listed in Table 1. Figure 7a shows the results for AOD(500). Derived profiles of Å(412/675) are presented in Figure 7b, where at each level the value relates to the column above. Values of K_{ext}(log scale) are shown in Figure 7c, derived using equation (2). Figure 7d shows profiles of geometric mean diameter of the particles in the range 60–1000 nm derived from the EC Ultra High Sensitivity Aerosol Spectrometer. Figure 7e shows high resolution profiles of CN (log scale), and Figure 7f are profiles of

BC derived from the SP2, shown in comparison with an averaged profile of BC from AGASP-I [*Hansen and Novakov*, 1989], and selected measurements from ground stations.

[36] The ensemble results shown in Figure 7 capture the general characteristics of the aerosol present in the Arctic during April 2009. As discussed above, most of the aerosol burden is attributed to emissions from industrial pollutants transported from Eurasia. Cleaner air at the beginning was sampled as it arrived over the Greenland ice cap from the Canadian Arctic (Figure 2a), and by 24/25 April at BRW there was long-range transport across Asia arriving from the North Pacific (Figure 2c). Such flow may have entrained dust and/or pollutants as it passed over the Asian continent, possibly volcanic aerosol as well; otherwise there was little evidence of distinct, elevated layers of dust or smoke during April 2009, in sharp contrast to conditions in the Alaskan Arctic during April 2008, when elevated smoke layers were observed [*Warneke et al.*, 2009]. There was, however, an enhancement of AOD at upper levels of the Arctic atmosphere compared with the tropics as evidenced in Figure 7a through a comparison with observations from MLO. Previous high-altitude evaluations of AOD at Arctic latitudes, including measurements made within the stratosphere, also revealed significantly lower values historically than observed in 2009 [*Herber et al.*, 2002; *Yamanouchi et al.*, 2005]. The reason for the 2009 enhancement is in part attributed to volcanic aerosols from the March eruptions of Mount Redoubt in Alaska, which will be discussed in section 3.6.

[37] Overall, during April 2009, a widely distributed and pervasive layer of haze blanketed much of the Arctic. Values of AOD(500) at times and places exceeded background conditions by a factor of six (Figure 5a) and were anomalously high compared with the prior three years (Figure 5b). The vertical structure of the haze is characterized as having systematically greater extinction toward the surface, within a shallow (665 m (±285)) surface-based temperature inversion (Figure 7c) and having a broad secondary peak between 1000 and 1500 m capping the inversion layer.

[38] The analysis of 15 Å(412/675) profiles (Figure 7b) indicates diminishing size of particles with increasing altitude that is corroborated by in situ measurements of geometric mean diameter (Figure 7d). Interestingly, the largest particles, on average, were found capping the inversion layer and correlates with the secondary peak in extinction. Above, as particles become smaller so does extinction. On the other hand, there is little if any correlation between CN concentration and extinction. This is evident by comparing Figure 7e with 7c. Note that both are plotted as log scales along the x axis to accentuate the orders of magnitude variations in these parameters. While CN varies by two orders of magnitude there are no monotonic changes with altitude. If any feature is notable it is the higher CN count above about 2 km where volume extinction diminishes significantly. That is, large CN concentrations do not necessarily result in higher extinction values, where CN concentration is a measure of the total number of particles. According to Mie theory, very small particles in the dispersion do not attenuate light efficiently. During the campaign, there was little evidence of distinct, optically thick aerosol layers above about 2.5 km in contrast with the smoky layers observed at the same time in 2008.

3.4. Black Carbon Measurements During PAM-ARCMIP

[39] Figure 7f shows 10 profiles of black carbon concentration, analyzed in a similar manner. In this case, data from individual profiles were averaged into 100 m layers and then the ensemble was averaged at 200 m resolution to match the other analyses; finally smoothing the ensemble mean.

[40] The measure of BC is especially important and has been a focus of many previous airborne campaigns in the Arctic, beginning in the 1980s with the Arctic Gas and Aerosol Sampling Program (AGASP) [*Schnell*, 1984; *Schnell et al.*, 1989]. Measurements of BC from a series of AGASP flights made in 1983 and 1986 were analyzed by *Hansen and Novakov* [1989]. Additional airborne observations made during the 2000 Arctic Study of Tropospheric Aerosol and Radiation (ASTAR) campaign verified the pervasiveness of black carbon at high latitudes [*Hara et al.*, 2003]. These observations caused alarm due to the high concentrations of soot, particularly at low tropospheric levels where particles absorb solar radiation, warm the planetary boundary layer and are thought to accelerate melting of snow and sea ice. Soot deposited on the surface was expected to reduce its albedo and further promote melt during late spring and summer. Twenty years later, there is still concern these processes pose a threat [e.g., *Flanner et al.*, 2007; *Clarke and Noone*, 2007; *Warneke et al.*, 2009], contributing to the decline in Arctic sea ice [*Stroeve et al.*, 2007].

[41] Measurements of BC made during PAM-ARCMIP are compared with historical observations to gain further perspective on the potential impacts of soot in the Arctic

Figure 7. Composite vertical profiles of (a) AOD(500), (b) Å(412/675), (c) $K_{ext}(\Delta z)$ (log scale), (d) geometric mean diameter, (e) CN concentration (log scale), and (f) BC concentration flown by the Polar-5 during PAM-ARCMIP. With exception of Figure 7f, each composite is comprised of the 15 profiles listed in Table 1 and shown by flight number in Figure 1 (map). Legends also give flight numbers and the nearest station identifier for cross reference with the map and Table 1. Note that NP-36 is highlighted by black dots and a thick orange line. The thicker black profiles are the average of each ensemble. Dashed lines indicate the ±1 standard deviation around respective means. The bold red curves are smoothed from the means to capture the main profile features. As discussed in the text, Figure 7a indicates the mean value of AOD(500) measured at an elevation of 3400 m at the NOAA Mauna Loa Observatory (MLO) during the first weeks of April 2009. Dashed horizontal lines indicate the average height of the surface-based temperature inversion, with ±1 standard deviation of heights indicated in Figure 7c by black diamonds. In Figure 7f, the bold black curve to the right is the average of seven profiles of BC measured during AGASP-I (adapted from *Hansen and Novakov* [1989]), and the black bars to the left represent the range of BC concentrations (±1 standard deviation around the mean) measured during April at Zeppelin Station in 2007 (Z07), at Barrow in 2007 (B07), and at Alert in 2008 (A08) for comparison.

environment. Figure 7f summarizes the profile data collected during April 2009 and compares it with an average of seven profiles collected during AGASP-I (adapted from *Hansen and Novakov* [1989, Figure 8]). *Hansen and Novakov* [1989] reported that "values (*of black carbon*) typically ranged from 300 to 500 ng m^{-3} at lower altitudes, deceasing gradually to 25 to 100 ng m^{-3} at 8–10 km." Results from PAM-ARCMIP show a range from 40 to 90 ng m^{-3} within the surface-based temperature inversion layer, decreasing monotonically to 30–50 ng m^{-3} at mid levels, and above 4 km, to less than 35 ng m^{-3}. The notable exception is the profile from NP-36 on 10 April, 2009. There, low-level values were a factor of five greater than the ensemble average but still only about 60% of typical values measured during the AGASP flights. It is important to note that during AGASP, BC was derived from filter samples collected using an Aethalometer calibrated following the method of *Gundel et al.* [1984]. Although claims were made that the Aethalometer was accurate to within 15–20%, there have been a number of studies that show that accuracy is dependent on assigning site-specific attenuation factors which also can vary seasonally [e.g., *Sharma et al.*, 2002; *Eleftheriadis et al.*, 2009]. The AGASP data are thus suspect. Derived values of BC may have been biased high if dust or other dark aerosols were also collected on filters during certain flight segments, however there is no way retrospectively to gage how much. During April, incursions of Asian dust do occur in the Arctic [*Stone et al.*, 2007, and references therein], however these tend to be episodic and were unlikely to have influenced all the AGASP I and II flights. Also, careful validations of Aethalometer BC retrievals have been made at Alert by *Sharma et al.* [2002] and at Zeppelin Station (464 m above NYA) by *Eleftheriadis et al.* [2009] that indicate the use of the manufacturer's recommended attenuation coefficient (k = 19 m^2 g^{-1}), at least during winter/spring, yields good results compared with those from a Particle Soot Absorption Photometer (PSAP) [e.g., *Sharma et al.*, 2002, Table 2]. Given the suspicious history of Aethalometer performance and its particular use here in the Arctic we speculate that the AGASP data shown in Figure 7f may be biased high, but probably not more than 30%. Still, the difference between the historic BC measurements and those from PAM-ARCMIP shown in Figure 7f are very significant and have climatic implications.

[42] Why the dramatic differences between 2009 and the 1980s? And are PAM-ARCMIP measurements representative of modern day conditions? Clues emerge when analyzing ground-based measurements of AOD and BC made at the Arctic observatories, BRW, ALT and NYA. *Bodhaine and Dutton* [1993] document a decrease in AOD during the spring months at BRW after 1982 that they attributed to decreasing industrial emissions in Europe and the former Soviet Union, the primary source region of Arctic haze [e.g., *Hirdman et al.*, 2010]. *Jaffe et al.* [1995] suggested that the observed trend may be related to variations in atmospheric circulation. The records of "equivalent" BC concentrations at BRW and ALT for the period 1989–2003 were later analyzed by *Sharma et al.* [2006]. They reported downward trends for the winter months of 54% at Alert and 33% at Barrow. A recent analysis of BC data collected from 1998 to 2007 at the Zeppelin Station by *Eleftheriadis et al.* [2009] established annual average and median values of 39 and 27 ng m^{-3}, respectively, with some indication of a continuing downward trend. Maximum values of ~80 ng m^{-3} were observed during winter, diminishing rapidly in late spring to ≤10 ng m^{-3} during the summer months.

[43] The Zeppelin values compare reasonably well with those at BRW and ALT reported by *Sharma et al.* [2006, Figure 2b]. The *Eleftheriadis et al.* [2009] values of 50–70 ng m^{-3} during April are also in good agreement with the low-level average derived from PAM-ARCMIP profiles. Recent values from these respective ground stations are shown in Figure 7f as black bars, defined by ±1 standard deviation around the mean. These independent assessments suggest that over the recent decades concentrations of BC in the Arctic atmosphere have stabilized at much lower values than were observed during the early 1980s. Values measured during PAM-ARCMIP, near the surface, are nearly an order of magnitude lower than estimated from AGASP data, if valid. *Sharma et al.* [2004, 2006], attribute the downward trends to decreased emissions of soot particles generated from fuel combustion, especially following the demise of the Soviet Union (December 1991), and changing circulation patterns that slowed the transport of pollutants into the Arctic from industrial regions.

[44] Further evidence of diminishing BC in the Arctic comes from a recently completed survey of soot (BC) concentrations measured in the annual snowpack. *Grenfell et al.* [2009] conducted the survey during the International Polar Year (IPY), during April/May of 2007 and 2008. They repeated measurements made in 1983–1984 [*Clarke and Noone*, 1985], extending coverage to eastern Russian and into the central Arctic. Results show a decline in soot in Arctic snow that is consistent with the 25-year downward trend in BC measured at Alert [*Quinn et al.*, 2007].

[45] Despite these encouraging assessments, it is apparent from the relative enhancement in BC at NP-36 on 10 April 2009, compared with all other PAM-ARCMIP profiles (Figure 7f), that there remains a rich source of soot that can be transported deep into the Arctic. In this instance, the source was most likely northern Russia as illustrated in Figure 2b. In general, conditions near the Pole were anomalous compared with other regions traversed by Polar-5. Referring to Figure 7a we see that AOD was relatively high at the surface and remained elevated at cruising altitude, indicating the presence of still higher aerosol layers. Values of Å(412/675) (Figure 7b) were very low, indicating the presence of relatively large particles in the column above cruising altitude, while only slightly larger particles were measured in the layer capping the inversion (Figure 7d). The values of Å(412/675) and geometric diameters are anti correlated, as would be expected. CN count was relatively low but variable through the entire column sampled (Figure 7e) and extinction was highly variable about the mean (Figure 7c) but shows fair correlation with BC concentrations at low levels. The higher concentration of black carbon within these layers probably absorbed solar radiation, while the larger particles increased scattering efficiency, combining to increase total extinction.

[46] While it is beyond the scope of this study to examine the details of individual profiles, it is apparent there is a wealth of information contained in the ensemble of data

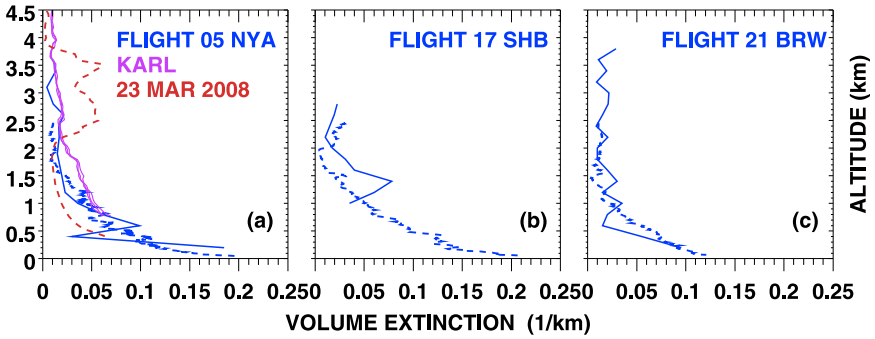

Figure 8. Comparison of extinction profiles derived from values of AOD(500) (Figure 7c) (solid blue curve) and those at 532 nm from the AMALi (dashed blue curve) in the vicinity of (a) NYA, (b) SCH, and (c) BRW (see also Figure 1 and Table 1). In addition, Figure 8a includes three retrievals (purple curve) made at 10 min intervals derived from the AWI KARL system operating coincidentally with aircraft operations nearby, and for a haze event (dashed red curve) that occurred on 23 March 2008.

collected during PAM-ARCMIP. The purpose of this first study was to introduce the data set and provide an overview of the main features that characterized the Arctic aerosol during April 2009. Additionally, limited but valuable comparative analyses were possible by combining the AOD-derived volume extinction profiles with various lidar-derived time-height cross-sections of extinction, described in the following section.

3.5. Lidar-Derived Extinction Compared With AOD-Derived Extinction Profiles

[47] AOD-derived extinction profiles are directly comparable with AMALi retrievals. Here, layer-averaged AOD was used to calibrate the AMALi data first and then 7.5 m-resolved profiles of extinction were derived. Because AMALi uses short integration times, 15 s (or equivalent to about a km in horizontal distance), and each pulse penetrates nearly to the surface, it is possible to obtain high resolution data, providing very detailed profiles of extinction. Results of three such comparisons are shown in Figure 8.

[48] Overall, the comparison between AOD-, AMALi- and KARL-derived extinction profiles for overlapping layers is quite reasonable considering their displacement in time and space and different vertical resolutions. As for the ensemble average of 15 profiles shown in Figure 7c, in each case, extinction derived from the lidar data increases toward the surface by nearly an order of magnitude below about 2 km, providing corroboration of the AOD-derived profiles. On 4 April, both the AOD and KARL results agree perfectly at the highest flight level at a time when AOD was very low (Figure 7a; Flight 05 NYA). No attenuating layers were observed in the upper troposphere at this time due to the influence of clean air flowing from Greenland. The 23 March, 2008 event (C. Ritter, manuscript in preparation, 2010), is in distinct contrast and provides an example of the kind of elevated aerosol layers that result from mid latitude source regions where aerosols are lofted and transported northward at higher altitudes.

[49] In past years, events similar to the 23 March case have occurred episodically throughout the Arctic, resulting from upper-level transport of pollutants from mid latitude sources. Such events include incursions of desert dust and smoke from biomass burning and forest fires [e.g., *Shaw*, 1982; *Stohl et al.*, 2006; *Stone et al.*, 2007], although it is unusual for smoke to be transported to the Arctic as early as April [*Warneke et al.*, 2009]. The opacity of the Arctic atmosphere varies dramatically over time and space, depending on emission rates, composition and transport processes [*Tomasi et al.*, 2007; *Quinn et al.*, 2007].

[50] Further evidence of the wide dispersion of Arctic haze, mostly in the lower boundary during April 2009, can be found in the archived images from CALIPSO at: http://www-calipso.larc.nasa.gov/products/lidar/browse_images/show_calendar.php. CALIPSO time-height cross sections nearly coincident with the Polar-5 flight track were examined. Each showed the presence of aerosol below about 2 km but rarely at upper levels of the troposphere. Images of the Kara Sea region and closer to the Russian industrial complexes also showed high concentrations of aerosol at low levels, providing further evidence of the pervasiveness of haze on a Pan-Arctic scale. CALIPSO images also reveal "stratospheric features" at altitudes between 8 and 12 km at high latitudes during April 2009, which are discussed in the following section.

3.6. Characterizing the Upper Atmosphere Aerosol During April 2009

[51] In Figure 7a one finds that AOD above 3400 m is relatively high, on average ~0.05. This is roughly an order of magnitude greater in value than that for the Arctic stratosphere [*Herber et al.*, 2002; *Thomason et al.*, 2003; *Yamanouchi et al.*, 2005]. The relative uniformity of AOD (500) indicated by the peaked frequency distribution in Figure 4f suggests a marked enhancement of the aerosol burden above 4 km. The significance of this feature emerges through a comparison with similar observations made at the NOAA Mauna Loa Observatory (MLO; 19.5°N, 155.6°W, elev. 3400 m). The average AOD(500) at MLO during the first weeks of April 2009 was ~0.026, whereas at the same altitude in the Arctic, AOD(500) ~0.055. Assuming a stratospheric background of 0.005, the free atmosphere above MLO had AOD(500) ≈0.02 compared with ≈0.05 in the Arctic. There are three plausible reasons for the apparent enhancement in AOD at high northern latitudes during this period, (1) a residual, upper tropospheric aerosol accumulated during late winter due to mid latitude pollutants, (2) the

presence of volcanic aerosols in the stratosphere and (3) intrusions of anthropogenic aerosol from a distant source, transported at stratospheric levels. Not having in situ observations above 4000 m we can only speculate on the role of each of these processes.

[52] 1. Most likely some of the upper-level aerosol burden is an accumulation of aged, long-lived aerosol of natural and anthropogenic origin, transported northward episodically from mid latitudes over the winter months, which become trapped within the Arctic vortex [e.g., *Quinn et al.*, 2007].

[53] 2. The stratospheric features that appear in the CALIPSO images may be volcanic in origin, widely dispersed plumes from the eruptions of Mount Redoubt in Alaska (60.49°N, 152.74°W). "Beginning Sunday March 22, 2009…, Redoubt Volcano produced a series of five explosive eruptions …., and AVO (Alaska Volcano Observatory) analysis of satellite imagery suggest that these events produced ash clouds that reached 60,000 ft above sea level…" (http://www.avo.alaska.edu/activity/Redoubt.php). Simulations made using the Environment Canada Lagrangian Particle Dispersion Model (http://eer.cmc.ec.gc.ca/people/Alain/eer/emergencies/Redoubt/Redoubt.html), and forward air trajectories originating from the volcano coordinates show an eastward and northward dispersion of effluents from Redoubt at high levels that appear to be drawn into the Arctic vortex during late March, early April. There was evidence of a volcanic plume in time-height cross-sections of aerosol backscatter collected at Eureka on 28 March using the AHSRL (E. Eloranta, private communication), and a few days later evident in the Ny-Ålesund KARL data. Volcanic gases, mostly SO_2, rising into the stratosphere can rapidly undergo gas-to-particle conversion to form very small sulfuric acid particles [e.g., *Hofmann and Rosen*, 1977; *Hofmann and Solomon*, 1989] that remain suspended for many months to years as they decay. Such injections can enhance the AOD of the stratosphere by 40–50 fold following major volcanic eruptions [*Stone et al.*, 1993], during which time cooling of the earth's surface may occur [*Dutton and Christy*, 1992].

[54] 3. A third possible source for stratospheric aerosol is from long-range transport of SO_2 gas emitted by coal-burning, mainly in China, which has been increasing over time. *Hofmann et al.* [2009] argue that, since 2000, an increase in sulfate aerosol in the stratosphere accounts for a 4–7% increase per year in stratospheric backscattering observed using lidar at MLO and Boulder, Colorado. This results when deep convection enhances the aerosol mass at high levels in the tropics. Once in the tropical stratosphere the aerosols can be dispersed globally; in the case of northward transport, via the Brewer-Dobson circulation [e.g., *Randel et al.*, 2006].

[55] We suspect that the enhancement in AOD observed in the Arctic during April 2009 is due to all three factors described here, although it is not possible to partition the individual contributions. Only after several years of monitoring, using a variety of platforms, will we determine if this feature persists, how variable it is and of what chemical make-up. Using lidar systems similar to those operating at Boulder and MLO, positioned at Arctic locations, in combination with CALIPSO, or succeeding space-borne lidar system, will we gain insight. Hopefully, subsequent airborne missions planned for future years will be part of this effort. Several high-altitude flight segments should be flown to better quantify the extinction by aerosols at high altitudes in the Arctic to better monitor changes in stratospheric AOD.

4. Discussion

[56] As of this writing, an advanced search of the World Wide Web, using Google, brings up 93,000 sites for "arctic haze" and only 7,150 for "arctic aerosols." The larger number of references to Arctic haze stems from the fact that so much of the literature focuses on this phenomenon. *Nordenskiöld* [1883] first raised interest after presenting evidence the Arctic was being contaminated by pollutants transported from lower latitudes. It was not until the 1970s, however, that focused studies commenced. Decades later there is still keen interest in Arctic aerosols because of their potential impacts on sea ice, which is in rapid decline [*Stroeve et al.*, 2007]. In general, "Arctic sea ice" is a hot topic on the Internet, with 477,000 Google references currently registered.

[57] The role of Arctic aerosols relative to variations in sea ice are not well understood. Some suggest that black carbon is contributing to Arctic warming and thus the demise of the pack ice through increased solar absorption by snow, darkened by soot, and/or BC within the atmosphere that enhances greenhouse warming. There are inadequate observations, however, to quantify these effects, or others that may lead to negative feedbacks (cooling).

[58] While not discussed previously, the indirect [*Twomey*, 1977] and semi-direct [e.g., *Stone et al.*, 2008] effects of aerosols on cloud microphysics and distributions can be significant. It appears that a reservoir of slightly larger particles may exist above the surface-based temperature inversion layer, which contributes to the higher volume extinction in that layer (Figure 7d and Figure 7c, respectively). The reason is not clear but may relate to aerosol-cloud interactions. Higher relative humidity is sometimes observed at this level so hygroscopic growth of the aerosol may occur, increasing particle size [*Herich et al.*, 2009]. Cloud formation and dissipation may occur if the air becomes super saturated and then dries, leading to possible perturbations in the particle size distribution. On the other hand, haze particles do not function effectively as ice nuclei IN. Even at −25 C, *Borys* [1989] found that pollutants tend to have very low IN/CN ratios and slow nucleation rates. These characteristics of Arctic haze tend to suppress wet deposition, which enables haze to survive long-range transport and accumulate within the Arctic atmosphere. It follows that ineffectual nucleation may suppress the deposition of soot onto the ice/snow surface. If ice crystals do not form readily and fall out, soot particles remain suspended in the stable atmosphere, unable to mix downward. It is later in the spring when the Arctic vortex breaks up that deposition can occur; that is when a supply of warmer moist air favors cloud formation and wet deposition and turbulent mixing as the inversion layer weakens. But at the same time Arctic air can be advected southward carrying suspended aerosols along isentropic surfaces that are ultimately scavenged and deposited to the surface. While it is certain that aerosols are removed from the Arctic atmosphere during the spring/summer transition, we cannot say what fraction of BC is deposited on snow or ice versus the amount removed by

advective processes. At Arctic ground stations, BC concentrations diminish rapidly in spring; e.g., at Barrow, the beginning of April and at Alert, by the middle of April [*Eleftheriadis et al.*, 2009]. Soot must either be deposited during these transitions, undetected as it mixes downward, or is transported away for the measuring sites. This is clearly a topic that requires additional study.

[59] Haze particles, composed mostly of sulfates, function as cloud condensation nuclei CCN if saturation occurs. Super cooled water clouds can form. Over the central ice pack, low-level clouds were seldom observed during the campaign due to an insufficient supply of moisture; few open leads were encountered and open water was distant. Near the surface, where there was open water and at the southern ice edge, sea smoke (fog) was observed from the aircraft [see supplemental material]. Low clouds of this type can have very significant radiative effects, involving competition between shortwave (SW) albedo and longwave (LW) thermal radiative forcing. Over the bright sea ice, LW effects probably dominate but over the dark ocean, SW forcing dominates. Differential heating of the atmosphere may result. In turn, there is a dynamical response in the wind field. This is only one example of the extraordinarily complex interactions that take place continually in the Arctic that makes modeling so difficult. In general, Arctic clouds tend to warm the surface under low solar illumination, but cool the surface under higher intensity light, especially over dark surfaces during summer [e.g., *Shupe and Intrieri*, 2004].

[60] As for April, 2009, the central Arctic was relatively dry, there were few low-level clouds and thus the effect of the haze was to cool the surface while warming (slightly) the layers above, through absorption and multiple reflections of sunlight. Because there were no measurements of the single scattering albedo ω_o made during PAM-ARCMIP, we cannot quantify the relative extinction by scattering and absorption. Historical observations made at BRW, however, can be used to infer values of ω_o, assuming that near-surface air represents the column (not always the case). At the surface, the mean value of ω_o at BRW for April (1988–2003) was ≈0.95, which shows an upward trend since 1988 [*Schnell et al.*, 2004, Figure 3.4]. That is, the near-surface air has become less absorbing in recent decades, a further indication that concentrations of soot in the Arctic atmosphere have decreased.

[61] This semi-direct effect of aerosol, the tendency for the atmosphere to warm while the surface is cooling, can suppress the formation of clouds. Depending on sun angle, surface albedo and the availability of moisture, the semi-direct effect of aerosols can enhance or diminish the direct forcing by aerosols, further complicating the task of quantifying the net climatic impact of Arctic aerosols. No attempt has been made here to quantify these very complicated interactions and feedbacks. On larger scales, *Rinke et al.* [2004] show how, via an aerosol-radiation-circulation feedback, the attenuation of sunlight by aerosols can induce changes in atmospheric pressure patterns that have the potential to modify teleconnections between the Arctic and lower latitudes.

[62] Empirical estimates of the direct radiative forcing by Arctic haze have been computed using the method developed by *Stone et al.* [2007, 2008]. Results for BRW (R. S. Stone et al., unpublished data, 2010) show that haze has approximately the same radiative forcing efficiency as Asia dust, and roughly twice that of boreal smoke (over snow). On this basis, a preliminary estimate of the direct radiative impact of the haze observed during PAM-ARCMIP can be made. For the range of AOD measured during the April 2009 campaign (Figure 4a and Figure 5a), we estimate daily net SW losses of ≈2–5 W m^{-2} during clear days, depending on the magnitude of AOD(500). Negative forcing of this magnitude would lead to a slight cooling of the surface. A number of early model studies provide estimates of direct shortwave radiative forcing by Arctic aerosols that are in this range [*Blanchet*, 1989, Table 2]. *Quinn et al.* [2007] calculated a value of ≈1 W m^{-2} for an AOD = 0.12 over snow having an albedo of 0.92. Aerosols over lower albedo surfaces, such as sea ice, will have a greater proportional effect [e.g., *Stone et al.*, 2008, Figure 10]. Incorporating aerosols into a regional climate model, *Treffeisen et al.* [2005] illustrate the sensitivity of forcing by aerosols to a wide range of Arctic conditions, which can lead to either heating or cooling at the surface. Without corroborating evidence we cannot determine if the negative forcing attibuted to the total atmospheric aerosol burden observed during April 2009 influenced the timing of melt onset, or if our results are representative climatologically.

[63] Recent changes in the Arctic climate can be attributed to a combination of natural variability, caused by changes in the large-scale dynamics that induce feedbacks in the coupled atmosphere-land-ice-ocean system, and warming due to the increasing concentrations of greenhouse gases in the atmosphere. Currently, simulations of future climate by ensembles of models reveal their largest discrepancies over the Arctic region, in part, due to the large uncertainty in quantifying the direct and indirect radiative effects of aerosols. In turn, there are large uncertainties as to how the Arctic influences the global climate on interannual to decadal time-scales because the energy exchanges within the global surface-atmosphere system are so difficult to model. Only through focused observational programs involving monitoring at ground stations, in conjunction with well-crafted aircraft campaigns and surveillance using satellites will we advance our understanding and develop more accurate parameterizations needed to improve climate predictions.

5. Summary and Conclusions

[64] The inaugural PAM-ARCMIP mission endeavored to characterize atmospheric aerosols by sampling over a vast region of the Arctic in a relatively short time, from the surface to mid tropospheric levels. It was a success, both scientifically and logistically. The acquisition of a unique, comprehensive, three-dimensional data set of aerosol optical depth was one of its achievements. Analyses of the data and ancillary measurements have been undertaken to provide an overview of conditions observed during April 2009 in the central Arctic.

[65] The analyses revealed some interesting features of Arctic aerosols during the peak of the 2009 haze season, highlighted below.

[66] 1. An evolving atmospheric circulation pattern (Figure 2) during the campaign caused the spatial variations observed in AOD(500); generally, airflow was dominant

from Eurasia, following pathways defined by 850 hPa geopotential and vector wind fields.

[67] 2. Arctic haze was pervasive but highly variable, having a bimodal frequency distribution (Figure 4); overall, values of AOD were anomalously high compared with the prior three years.

[68] 3. Peak values of AOD(500) exceeded 0.35 in the Beaufort Sea region toward the end of April, compared with background values of ≤0.06 (Figure 5); long-range transport of a variety of aerosols was implicated (Figure 2c).

[69] 4. Vertical structure was also highly variable but, on average, showed the greatest extinction near the surface, decreasing through the surface-based temperature inversion layer, having a secondary peak above, and diminishing aloft (Figure 7c).

[70] 5. There were few turbid layers above 2.5 km, rather a general enhancement in AOD at upper levels compared with similar data collected at a tropical site (Figure 7a) or during previous Arctic campaigns; the Arctic enhancement is attributed to a combination of residual, aged aerosol, possible contribution from coal burning in China, and volcanic aerosol from the March/April volcanic eruptions of Mount Redoubt in Alaska.

[71] 6. The haze was composed of moderately small particles having diameters in the range 130–200 nm (Figure 7d), largest in a layer capping the inversion layer and diminishing with height; derivations of Å(412/675) provided further evidence of diminishing particle size with increasing altitude.

[72] 7. CN concentrations were highly variable and revealed no relationship to volume extinction or particle size (Figures 7e and 7c).

[73] 8. BC concentrations were relatively low during the campaign, with the exception of samples collected near North Pole; values near the surface were nearly an order of magnitude lower than values reported from similar campaigns in the 1980s.

[74] 9. Concentrations of BC measured at the lowest atmospheric levels during PAM-ARCMIP match reasonably well with in situ measurements made at ground stations throughout the Arctic in recent years (Figure 7f), sites where BC has been in decline since the late 1980s [*Sharma et al.*, 2006; *Quinn et al.*, 2007; *Eleftheriadis et al.*, 2009].

[75] 10. Owing to relatively low BC concentrations near the surface, and inhibited by an omnipresent surface-based temperature inversion layer during April 2009, deposition of soot to the surface was probably minimal, a condition that may underlie the downward trends in soot measured in the Arctic snowpack [*Grenfell et al.*, 2009].

[76] 11. The aerosols observed in the Arctic during April 2009 acted to attenuate sunlight, resulting in a slight cooling of the surface; a finding consistent with previous empirical studies as well as model simulations of the direct radiative impact of aerosols in the Arctic.

[77] Airborne campaigns devoted to the study of the aerosol are valuable, providing snapshots in time and space from which to characterize aerosols and assess their climate impacts. With appropriate international interest and support, the plan is to repeat the PAM-ARCMIP mission twice a year, during spring and late summer, roughly at the times of sea ice maximum and minimum, which coincidently occur during the most and least turbid times of year in the Arctic. As soon as logistical barriers are overcome, the plan is to fly circum navigations of the entire Arctic with strategic operations from Siberian stations along the route. In conjunction with observations made at the network of Arctic climate observatories, aircraft measurements will enable further verification of regional climate models and for the validation of satellite retrievals of surface and atmospheric properties.

[78] **Acknowledgments.** PAM-ARCMIP was a success thanks to behind-the-scenes efforts by many individuals from the participating institutes and affiliates. Those of us who flew the mission wish to express special thanks to B. Burchartz and his crew for piloting Polar-5, flight engineers M. Gehrmann and M. Sellmann, and others at AWI responsible for integrating the systems into the aircraft. W. Strapp operated the EC suite of instruments on the final legs of the mission. R. Brauner provided accurate weather forecasts. S. Henkel handled administrative matters. We thank the crew of the Russian North-Pole drifting station NP-36 and logistic head, V. T. Sokolov of the Arctic and Antarctic Research Institute (AARI), St. Petersburg for assuring our safe landing there and their hospitality. Personnel at ground stations across the Arctic provided for our needs, especially A. Platt and J. Johns. Logistical support was also provided by the U.S. DOE/ARM program, the Barrow Arctic Science Consortium (BASC) and Arctic Kingdom. Assistance with data processing and access to data were provided by D. Longenecker, J. Harris, S. Debatin, J. Graeser, and the crew of NP-35. B. Holben, C. Toledano, and K. Stebel provided the ancillary AOD data used in Figure 5. S. Sharma and K. Eleftheriadis provided the station BC results used in Figure 7f. J. Wendell assisted with the fabrication of the photometer system. K.-H. Schulz provided the solar tracker. P. Disterhoft assisted with characterization of the special glass window. N. O'Neill and E. Eloranta provided ancillary analyses used in the interpretation of lidar data. T. Grenfell provided insights about BC trends in the Arctic. NCEP gridded data was made available through the NOAA ESRL Physical Sciences Division. C. Tomasi provided support and encouragement through the Polar-AOD IPY project, and also sponsored the development of the NOAA ISAC Sun photometer used during PAM-ARMIP. In part, this study was supported by the Italian National Research Council (CNR) through its Short-term Mobility Programme and with funds provided by NOAA/ESRL. R. Stone dedicates his contribution to this study to the late David Hofmann, who, during his tenure at NOAA, provided critical support and enduring inspiration. Dave was keenly interested in PAM-ARCMIP, having earlier cosponsored the development of the Sun photometer system used during the campaign.

References

Alexandrov, M. D., A. Marshak, B. Cairns, A. A. Lacis, and B. E. Carlson (2004), Automated cloud screening algorithm for MFRSR data, *Geophys. Res. Lett.*, *31*, L04118, doi:10.1029/2003GL019105.

Ångström, A. (1929), On the atmospheric transmission of Sun radiation and on dust in the air, *Geogr. Ann.*, *11*, 156–166, doi:10.2307/519399.

Ångström, A. (1964), The parameters of atmospheric turbidity, *Tellus*, *16*, 64–75, doi:10.1111/j.2153-3490.1964.tb00144.x.

Ansmann, A., U. Wandinger, M. Riebesell, C. Weitkamp, and W. Michaelis (1992), Independent measurement of extinction and backscatter profiles in cirrus clouds by using a combined Raman elastic-backscatter lidar, *Appl. Opt.*, *31*, 7113, doi:10.1364/AO.31.007113.

Arnold, F., R. Nau, T. Jurkat, H. Schlager, A. Minikin, A. Dörnbrack, L. Pirjola, and A. Stohl (2009), Central Arctic Atmospheric SO_2 pollution from smelters: Airborne detection and Arctic Haze formation, *Geophys. Res. Abstr.*, *11*, Abstract EGU2009–3560–1.

Balis, D., M. Kroon, M. E. Koukouli, E. J. Brinksma, G. Labow, J. P. Veefkind, and R. D. McPeters (2007), Validation of Ozone Monitoring Instrument total ozone column measurements using Brewer and Dobson spectrophotometer ground-based observations, *J. Geophys. Res.*, *112*, D24S46, doi:10.1029/2007JD008796.

Berk, A., et al. (2004), MODTRAN5: A reformulated atmospheric band model with auxiliary species and practical multiple scattering options, *Proc. SPIE Int. Soc. Opt. Eng.*, *5571*, 78–85.

Blanchet, J.-P. (1989), Toward estimation of climatic effects due to Arctic aerosols, *Atmos. Environ.*, *23*, 2609–2625, doi:10.1016/0004-6981(89)90269-2.

Bodhaine, B. A., and E. G. Dutton (1993), A long-term decrease in Arctic haze at Barrow, Alaska, *Geophys. Res. Lett.*, *20*(10), 947–950, doi:10.1029/93GL01146.

Borys, R. D. (1989), Studies of ice nucleation by Arctic aerosol on AGASP-II, *J. Atmos. Chem.*, *9*, 169–185, doi:10.1007/BF00052831.

Cai, Y., D. C. Montague, W. Mooiweer-Bryan, and T. Deshler (2008), Performance characteristics of the ultra high sensitivity aerosol spectrometer for particles between 55 and 800 nm: Laboratory and field studies, *J. Aerosol Sci.*, *39*, 759–769, doi:10.1016/j.jaerosci.2008.04.007.

Celarier, E. A., et al. (2008), Validation of Ozone Monitoring Instrument nitrogen dioxide columns, *J. Geophys. Res.*, *113*, D15S15, doi:10.1029/2007JD008908.

Clarke, A. D., and K. J. Noone (1985), Soot in the arctic snowpack: A cause for perturbations in radiative transfer, *Atmos. Environ.*, *19*, 2045–2053.

Clarke, A. D., and K. J. Noone (2007), Soot in the arctic snowpack: A cause for perturbations in radiative transfer, *Atmos. Environ.*, *41*, 64–72, doi:10.1016/j.atmosenv.2007.10.059.

Dutton, E. G., and J. R. Christy (1992), Solar radiative forcing at selected locations and evidence for global lower tropospheric cooling following the eruptions of El Chichón and Pinatubo, *Geophys. Res. Lett.*, *19*(23), 2313–2316, doi:10.1029/92GL02495.

Dutton, E. G., J. J. Deluisi, and G. Herbert (1989), Shortwave aerosol optical depth of Arctic haze measured on board the NOAA WP-3D during AGASP-II, April 1986, *J. Atmos. Chem.*, *9*, 71–79, doi:10.1007/BF00052825.

Eleftheriadis, K., S. Vratolis, and S. Nyeki (2009), Aerosol black carbon in the European Arctic: Measurements at Zeppelin station, Ny-Ålesund, Svalbard from 1998–2007, *Geophys. Res. Lett.*, *36*, L02809, doi:10.1029/2008GL035741.

Eloranta, E. W. (2005), High spectral resolution lidar, in *Lidar: Range-Resolved Optical Remote Sensing of the Atmosphere*, edited by K. Weitkamp, pp. 143–163, Springer, New York.

Flanner, M. G., C. S. Zender, J. T. Randerson, and P. J. Rasch (2007), Present-day climate forcing and response from black carbon in snow, *J. Geophys. Res.*, *112*, D11202, doi:10.1029/2006JD008003.

Grenfell, T. C., S. G. Warren, V. F. Radionov, V. N. Makarov, and S. A. Zimov (2009), Expeditions to the Russian Arctic to survey black carbon in snow, *Eos Trans. AGU*, *90*(43), 386, doi:10.1029/2009EO430002.

Gundel, L. A., R. L. Dod, H. Rosen, and T. Novakov (1984), The relationship between optical attenuation and black carbon concentration for ambient and source particles, *Sci. Total Environ.*, *36*, 197–202, doi:10.1016/0048-9697(84)90266-3.

Hansen, A. D. A., and T. Novakov (1989), Aerosol black carbon measurements in the Arctic haze during AGASP-II, *J. Atmos. Chem.*, *9*, 347–361, doi:10.1007/BF00052842.

Hara, K., S. Yamagata, T. Yamanouchi, K. Sato, A. Herber, Y. Iwasaka, M. Nagatani, and H. Nakata (2003), Mixing states of individual aerosol particles in spring Arctic troposphere during ASTAR 2000 campaign, *J. Geophys. Res.*, *108*(D7), 4209, doi:10.1029/2002JD002513.

Herber, A., L. W. Thomason, H. Gernandt, U. Leiterer, D. Nagel, K.-H. Schulz, J. Kaptur, T. Albrecht, and J. Notholt (2002), Continuous day and night aerosol optical depth observations in the Arctic between 1991 and 1999, *J. Geophys. Res.*, *107*(D10), 4097, doi:10.1029/2001JD000536.

Herich, H., L. Kammermann, B. Friedman, D. S. Gross, E. Weingartner, U. Lohmann, P. Spichtinger, M. Gysel, U. Baltensperger, and D. J. Cziczo (2009), Subarctic atmospheric aerosol composition: 2. Hygroscopic growth properties, *J. Geophys. Res.*, *114*, D13204, doi:10.1029/2008JD011574.

Hirdman, D., H. Sodemann, S. Eckhardt, J. F. Burkhart, A. Jefferson, T. Mefford, P. K. Quinn, S. Sharma, J. Ström, and A. Stohl (2009), Source identification of short-lived air pollutants in the Arctic using statistical analysis of measurement data and particle dispersion model output, *Atmos. Chem. Phys. Discuss.*, *9*, 19,879–19,937, doi:10.5194/acpd-9-19879-2009.

Hirdman, D., H. Sodemann, S. Eckhardt, J. F. Burkhart, A. Jefferson, T. Mefford, P. K. Quinn, S. Sharma, J. Ström, and A. Stoh (2010), Source identification of short-lived air pollutants in the Arctic using statistical analysis of measurement data and particle dispersion model output, *Atmos. Chem. Phys.*, *10*, 669–693, doi:10.5194/acp-10-669-2010.

Hoffmann, A., C. Ritter, M. Stock, M. Shiobara, A. Lampert, M. Maturilli, T. Orgis, R. Neuber, and A. Herber (2009), Ground-based lidar measurements from Ny-Ålesund during ASTAR 2007, *Atmos. Chem. Phys. Discuss.*, *9*, 15,453–15,510, doi:10.5194/acpd-9-15453-2009.

Hofmann, D. J., and J. M. Rosen (1977), Balloon observations of the time development of the stratospheric aerosol event of 1974–1975, *J. Geophys. Res.*, *82*(9), 1435–1440, doi:10.1029/JC082i009p01435.

Hofmann, D. J., and S. Solomon (1989), Ozone destruction through heterogeneous chemistry following the eruption of El Chichón, *J. Geophys. Res.*, *94*(D4), 5029–5041, doi:10.1029/JD094iD04p05029.

Hofmann, D., J. Barnes, M. O'Neill, M. Trudeau, and R. Neely (2009), Increase in background stratospheric aerosol observed with lidar at Mauna Loa Observatory and Boulder, Colorado, *Geophys. Res. Lett.*, *36*, L15808, doi:10.1029/2009GL039008.

Holben, B. N., et al. (1998), AERONET—A federated instrument network and data archive for aerosol characterization, *Remote Sens. Environ.*, *66*(1), 1–16, doi:10.1016/S0034-4257(98)00031-5.

Intergovernmental Panel on Climate Change (2007), *Climate Change 2007: The Physical Science Basis. Summary for Policy Makers. Contribution of Working Group I to the Fourth Assessment Report of the Intergovernmental Panel on Climate Change*, Cambridge Univ. Press, Cambridge, U. K.

Jaffe, D., T. Iversen, and G. Shaw (1995), Comment on "A long term decrease in arctic haze at Barrow, Alaska" by B. A. Bodhaine and E. G. Button, *Geophys. Res. Lett.*, *22*(6), 739–740, doi:10.1029/95GL00567.

Kaufman, Y. J., and R. S. Fraser (1997), The effect of smoke particles on clouds and climate forcing, *Science*, *277*, 1636, doi:10.1126/science.277.5332.1636.

Kaufman, Y. J., A. Gitelson, A. Karnieli, E. Ganor, R. S. Fraser, T. Nakajima, S. Mattoo, and B. N. Holben (1994), Size distribution and scattering phase function of aerosol particles retrieved from sky brightness measurements, *J. Geophys. Res.*, *99*(D5), 10,341–10,356, doi:10.1029/94JD00229.

Mazzola, M., C. Lanconelli, A. Lupi, M. Busetto, V. Vitale, and C. Tomasi (2010), Columnar aerosol optical properties in the Po Valley, Italy, from MFRSR data, *J. Geophys. Res.*, doi:10.1029/2009JD013310, in press.

Mitchell, J. M. (1957), Visual range in the polar regions with particular reference to the Alaskan Arctic, *J. Atmos. Terr. Phys.*, *17*, 195–211.

Nordenskiöld, A. E. (1883), Nordenskiöld on the inland ice of Greenland, *Science*, *2*, 732–738, doi:10.1126/science.ns-2.44.732.

O'Neill, N. T., O. Dubovik, and T. F. Eck (2001), Modified Ångström exponent for the characterization of submicrometer aerosols, *Appl. Opt.*, *40*, 2368–2375, doi:10.1364/AO.40.002368.

Quinn, P. K., G. Shaw, E. Andrews, E. G. Dutton, T. Ruoho-Airola, and S. L. Gong (2007), Arctic haze: Current trends and knowledge gaps, *Tellus, Ser. B*, *59*, 99–114, doi:10.1111/j.1600-0889.2006.00238.x.

Raatz, W. E. (1989), An anticyclone point of view on low-level tropospheric long-range transport, *Atmos. Environ.*, *23*, 2501–2504, doi:10.1016/0004-6981(89)90261-8.

Randel, W. J., F. Wu, H. Vömel, G. E. Nedoluha, and P. Forster (2006), Decreases in stratospheric water vapor after 2001: Links to changes in the tropical tropopause and the Brewer-Dobson circulation, *J. Geophys. Res.*, *111*, D12312, doi:10.1029/2005JD006744.

Rinke, A., K. Dethloff, and M. Fortmann (2004), Regional climate effects of Arctic Haze, *Geophys. Res. Lett.*, *31*, L16202, doi:10.1029/2004GL020318.

Rinke, A., et al. (2006), Evaluation of an ensemble of Arctic regional climate models: Spatiotemporal fields during the SHEBA year, *Clim. Dyn.*, *26*, 459–472, doi:10.1007/s00382-005-0095-3.

Russell, P., et al. (2005), Aerosol optical depth measurements by airborne Sun photometer in SOLVE II: Comparisons to SAGE III, POAM III and airborne spectrometer measurements, *Atmos. Chem. Phys.*, *5*, 1311–1339, doi:10.5194/acp-5-1311-2005.

Saha, A., et al. (2010), Pan-Arctic sunphotometry during the ARCTAS-A campaign of April 2008, *Geophys. Res. Lett.*, *37*, L05803, doi:10.1029/2009GL041375.

Schnell, R. C. (1984), Arctic haze and the Arctic Gas and Aerosol Sampling Program (AGASP), *Geophys. Res. Lett.*, *11*(5), 361–364, doi:10.1029/GL011i005p00361.

Schnell, R. C., T. B. Watson, and B. A. Bodhaine (1989), NOAA WP-3D instrumentation and flight operations on AGASP-II, *J. Atmos. Chem.*, *9*, 3–16, doi:10.1007/BF00052822.

Schnell, R. C., et al. (Eds.) (2004), Climate Monitoring and Diagnostics Laboratory summary report 27: 2002–2003, report, 174 pp., CMDL, Boulder, Colo.

Sharma, S., J. R. Brook, H. Cachier, J. Chow, A. Gaudenzi, and G. Lu (2002), Light absorption and thermal measurements of black carbon in different regions of Canada, *J. Geophys. Res.*, *107*(D24), 4771, doi:10.1029/2002JD002496.

Sharma, S., D. Lavoué, H. Cachier, L. A. Barrie, and S. L. Gong (2004), Long-term trends of the black carbon concentrations in the Canadian Arctic, *J. Geophys. Res.*, *109*, D15203, doi:10.1029/2003JD004331.

Sharma, S., E. Andrews, L. A. Barrie, J. A. Ogren, and D. Lavoué (2006), Variations and sources of the equivalent black carbon in the high Arctic revealed by long-term observations at Alert and Barrow: 1989–2003, *J. Geophys. Res.*, *111*, D14208, doi:10.1029/2005JD006581.

Shaw, G. E. (1982), Evidence for a central Eurasian source area of Arctic haze in Alaska, *Nature*, *299*, 815–818, doi:10.1038/299815a0.

Shaw, G. E. (1995), The Arctic haze phenomenon, *Bull. Am. Meteorol. Soc.*, *76*, 2403–2413, doi:10.1175/1520-0477(1995)076<2403:TAHP>2.0.CO;2.

Shaw, G. E., and K. Stamnes (1980), Arctic haze: Perturbation of the polar radiation budget, *Ann. N. Y. Acad. Sci.*, *338*, 533–540, doi:10.1111/j.1749-6632.1980.tb17145.x.

Shiobara, M., Y. Fujii, S. Morimoto, Y. Asuma, S. Yamagata, S. Sugawara, Y. Inomata, M. Watanabe, and T. Machida (1999), An overview and preliminary results from the Arctic Airborne Measurement Program 1998 campaign, *Polar Meteorol. Glaciol.*, *13*, 99–110.

Shupe, M. D., and J. M. Intrieri (2004), Cloud radiative forcing of the Arctic surface: The influence of cloud properties, surface albedo, and solar zenith angle, *J. Clim.*, *17*(3), 616–628, doi:10.1175/1520-0442(2004)017<0616:CRFOTA>2.0.CO;2.

Skouratov, S. (1997), Vertical profiles of arctic haze aerosol in spring 1994 obtained by using spectrophotometric measurements, *Atmos. Res.*, *44*(1–2), 113–124, doi:10.1016/S0169-8095(97)00005-7.

Slowik, J. G., et al. (2007), An inter-comparison of instruments measuring black carbon content of soot particles, *Aerosol Sci. Technol.*, *41*(3), 295–314, doi:10.1080/02786820701197078.

Spinhirne, J. D., and M. D. King (1985), Latitudinal variation of spectral optical thickness and columnar size distribution of the El Chichon stratospheric aerosol layer, *J. Geophys. Res.*, *90*(D6), 10,607–10,619, doi:10.1029/JD090iD06p10607.

Stachlewska, I. S., R. Neuber, A. Lampert, C. Ritter, and G. Wehrle (2009), Amali—the Airborne Mobile Aerosol Lidar for Arctic research, *Atmos. Chem. Phys. Discuss.*, *9*, 18,745–18,792, doi:10.5194/acpd-9-18745-2009.

Stohl, A., et al. (2006), Pan-Arctic enhancements of light absorbing aerosol concentrations due to North American boreal forest fires during summer 2004, *J. Geophys. Res.*, *111*, D22214, doi:10.1029/2006JD007216.

Stone, R. S. (2002), Monitoring aerosol optical depth at Barrow, Alaska and South Pole: Historical overview, recent results, and future goals, in *Proceedings of the 9th Workshop Italian Research on Antarctic Atmosphere*, edited by M. Colacino, pp. 123–144, Ital. Phys. Soc., Bologna, Italy. (Available at http://www.cmdl.noaa.gov/hotitems/Porano9EXTabs.pdf)

Stone, R. S., J. R. Key, and E. G. Dutton (1993), Properties and decay of stratospheric aerosols in the Arctic following the 1991 eruptions of Mount Pinatubo, *Geophys. Res. Lett.*, *20*(21), 2359–2362, doi:10.1029/93GL02684.

Stone, R. S., G. P. Anderson, E. Andrews, E. G. Dutton, E. P. Shettle, and A. Berk (2007), Incursions and radiative impact of Asian dust in northern Alaska, *Geophys. Res. Lett.*, *34*, L14815, doi:10.1029/2007GL029878.

Stone, R. S., G. P. Anderson, E. P. Shettle, E. Andrews, K. Loukachine, E. G. Dutton, C. Schaaf, and M. O. Roman III (2008), Radiative impact of boreal smoke in the Arctic: Observed and modeled, *J. Geophys. Res.*, *113*, D14S16, doi:10.1029/2007JD009657.

Stroeve, J., M. M. Holland, W. Meier, T. Scambos, and M. Serreze (2007), Arctic sea ice decline: Faster than forecast, *Geophys. Res. Lett.*, *34*, L09501, doi:10.1029/2007GL029703.

Thomason, L. W., A. B. Herber, T. Yamanouchi, and K. Sato (2003), Arctic Study on Tropospheric Aerosol and Radiation: Comparison of tropospheric aerosol extinction profiles measured by airborne photometer and SAGE II, *Geophys. Res. Lett.*, *30*(6), 1328, doi:10.1029/2002GL016453.

Tomasi, C., et al. (2007), Aerosols in polar regions: A historical overview based on optical depth and in situ observations, *J. Geophys. Res.*, *112*, D16205, doi:10.1029/2007JD008432.

Treffeisen, R., A. Rinke, M. Fortmann, K. Dethloff, A. Herber, and T. Yamanouchi (2005), A case study of the radiative effects of Arctic aerosols in March 2000, *Atmos. Environ.*, *39*, 899–911, doi:10.1016/j.atmosenv.2004.09.066.

Treffeisen, R., et al. (2007), Arctic smoke—Aerosol characteristics during a record air pollution event in the European Arctic and its radiative impact, *Atmos. Chem. Phys.*, *7*, 3035–3053, doi:10.5194/acp-7-3035-2007.

Twomey, S. (1977), The influence of pollution on the shortwave albedo of clouds, *J. Atmos. Sci.*, *34*, 1149–1152, doi:10.1175/1520-0469(1977)034<1149:TIOPOT>2.0.CO;2.

Uttal, T., et al. (2002), Surface heat budget of the Arctic Ocean, *Bull. Am. Meteorol. Soc*, *83*, 255–275, doi:10.1175/1520-0477(2002)083<0255:SHBOTA>2.3.CO;2.

Warneke, C., et al. (2009), Biomass burning in Siberia and Kazakhstan as an important source for haze over the Alaskan Arctic in April 2008, *Geophys. Res. Lett.*, *36*, L02813, doi:10.1029/2008GL036194.

Yamanouchi, T., et al. (2003), Preliminary report of the "Arctic Airborne Measurement Program 2002" (AAMP 02), *Polar Meteorol. Glaciol.*, *17*, 103–115.

Yamanouchi, T., et al. (2005), Arctic Study of Tropospheric Aerosol and Radiation (ASTAR) 2000: Arctic haze case study, *Tellus, Ser. B*, *57*, 141–152, doi:10.1111/j.1600-0889.2005.00140.x.

K. Dethloff, M. Maturilli, R. Neuber, C. Ritter, and M. Stock, Research Unit Potsdam, Alfred Wegener Institute for Polar and Marine Research, Am Telegrafenberg A 43, D-14473 Potsdam, Germany.

E. G. Dutton, R. C. Schnell, and R. S. Stone, Global Monitoring Division, Earth Systems Research Laboratory, National Oceanic and Atmospheric Administration, 325 Broadway, Boulder, CO 80305, USA. (Robert.Stone@noaa.gov)

A. Herber, Climate Sciences, Alfred Wegener Institute for Polar and Marine Research, Am Alten Hafen 26, D-27568 Bremerhaven, Germany.

A. Lampert, Institute of Aerospace Systems, Technische Universität Braunschweig, Hermann-Blenk-Str. 23, D-38108 Braunschweig, Germany.

S.-M. Li, Air Quality Research Division, Science and Technology Branch, Environment Canada, 4905 Dufferin St., Toronto, ON M3H 5T4, Canada.

P. S. K. Liu, Meteorological Research Division, Environment Canada, 4905 Dufferin St., Toronto, ON M3H 5T4, Canada.

A. Lupi, M. Mazzola, and V. Vitale, Institute of Atmospheric Sciences and Climate, National Research Council, Via Gobetti 101, I-40129 Bologna, Italy.